RÉPUBLIQUE FRANÇAISE
Liberté
Égalité
Fraternité

ONERA
THE FRENCH AEROSPACE LAB

SC539 - Aerosol Light-scattering for Lidar Remote-sensing

An introduction course

Romain Ceolato

Sunday, 19 October 2025 - Prague, Czech Republic

[1] ONERA, [2] Toulouse University

Objectives

This short-course discusses both fundamentals and applications of light-scattering for lidar and remote-sensing. It gives an introduction to the field of light-scattering by particles, including soot and smoke aerosols.

Outline

1. Introduction

Introduction

- Elastic backscatter lidar is an active optical remote-sensing technique for range-resolved monitoring of aerosols, providing quantitative information about aerosol-particle properties. This is crucial for environmental science, air quality monitoring, climate change assessment, and space-based studies of planetary atmospheres [1, 2, 3, 4, 5].
- Lidar relies on light-scattering, and for *elastic* lidar, the wavelength remains unchanged during scattering.
- Early systems from the 1930s used incoherent flash lamps to sense atmospheric constituents [6, 7, 8]. The advent of lasers in the 1960s significantly enhanced the resolution of atmospheric aerosol profiles [9, 10, 11].
- The principle is simple : laser pulses travel through the atmosphere, and a sensor near the laser detects the backscattered light from particles or gas molecules [12, 13]. Thus, lidar provides range-resolved measurements of aerosol distribution.

Introduction

- Techniques employing light scattering, such as lidar, can characterize micron-scale and smaller particulate matter in a contact-free manner, making it useful for aerosols where collecting particle samples is impractical or impossible.
- By measuring how incident light disperses in angle upon scattering from a particle, a variety of particle-relevant characteristics can be estimated, provided that a suitable model is available to connect the pattern to these characteristics.
- One such model is Mie theory, developed in 1908, which is the analytical solution to the Maxwell equations for scattering by a homogeneous spherical particle of radius R and complex-valued refractive index m illuminated by a plane electromagnetic wave.

Introduction (cont.)

- Mie theory involves expanding the incident plane wave and the sphere's internal and scattered waves as infinite series of vector spherical harmonics, linked by the boundary conditions at the sphere surface.
- Mie theory is popular for calculating the radiative properties of aerosol particles, including backscattering and extinction cross-sections, and is applied to derive the Optical Properties of Aerosols and Clouds (OPAC) data set, widely used in the remote-sensing community.
- However, Mie theory is invalid for non-liquid drop aerosol particles, such as mineral dust, soot, volcanic ash, and ice, as their morphology is poorly represented as spheres. Applying Mie theory in such cases can induce significant inaccuracies in the interpretation of lidar measurements.

Advanced Light-Scattering Techniques

- Recent work focuses on investigating the light-scattering properties of non-spherical aerosol particles.
- If such particles are homogeneous in composition and axially symmetric in shape, the T-matrix method becomes applicable.
- This solution to the Maxwell equations is attributed to Waterman [14] and is reviewed by Mishchenko [15, 16].
- The incident and scattered waves are related via the transition matrix, or simply "T-matrix," which depends only on the properties of a particle and the choice of coordinate system, but not on the incident wave.
- The T-matrix method is used in a variety of situations of interest to atmospheric aerosols, including fractal-like soot aggregates [17, 18] and is usually efficient for computing the radiative properties of ensembles of randomly oriented particles.

Advanced Light-Scattering Techniques

- For more irregularly-shaped particles, i.e., those without symmetry, and particles with inhomogeneous composition, more flexible solutions are required.
- One such solution is the Discrete Dipole Approximation (DDA).
- The DDA, which is based on the volume integral equation solution to the Maxwell equations, is attributed to Purcell et al. [19] and reviewed by Draine [20] and Yurkin et al. [21].
- The DDA represents the volume of an arbitrary shaped particle by a finite array of point electric dipoles each with their own polarizability placed on a cubic lattice.
- The array of dipoles respond to an incident wave, interact with each other, and collectively radiate to constitute the particle's scattered wave.
- Due to the ability to model scattering from any particle shape and handle particle inhomogeneity, the DDA offers perhaps the greatest flexibility for a solution to the Maxwell equations, although at the cost of potentially time-consuming computation [21, 22, 23]

Advanced Light-Scattering Techniques

- Accurate models of aerosol properties (particle-size distributions, refractive index, particle shape) are essential for inferring quantitative information from lidar signals.
- Important quantities : aerosol backscatter and extinction cross sections (C^{bac} and C^{ext}) determined by particle properties.
- Wood et al. [24] studied the backscattering coefficient as a function of wavelength to identify the chemical composition of atmospheric aerosols.
- Determining particle size distribution from aerosol backscattering and extinction coefficients demonstrated using multiple wavelengths [25, 26].
- Extensive work on retrieving particle size distribution [27, 28, 29, 30, 31, 32, 33, 34] and refractive index [35, 36, 37].

Polarization Sensitive Techniques

- Polarization sensitive techniques improve aerosol and cloud characterization, particularly regarding particle shape [38, 39].
- Polarimetric elastic lidar distinguishes spherical from irregularly shaped particles via depolarization measurements [40, 41].
- Applied to clouds, it can distinguish ice clouds from water clouds [42].
- Identifies and discriminates different types of aerosols : volcanic ash [43], dust [44], black carbon [45], contrails [46], biological warfare agents [47].
- Single wavelength measurements (e.g., linear depolarization ratio of dust [40]) and multiple wavelengths show ability to distinguish different types of aerosols [48, 49, 37, 50, 51, 52, 45].

Problem Statement : Lidar Inversion

- Evaluating aerosol extinction and backscattering properties is challenging in elastic backscatter lidar applications.
- The elastic lidar equation must be inverted to infer aerosol properties, but lidar inversion is an ill-posed problem.
- Several atmospheric conditions can lead to the same lidar return signal, requiring additional information for accurate inversion.
- Additional information can come from prior knowledge, light-scattering simulations, or other instruments (e.g., sunphotometers, particle counters).

2. Elastic Lidar Theory

Elastic Lidar Theory

- Pulses emitted from a lidar interact with atmosphere constituents, namely aerosol particles and gas molecules.
- The interactions include the absorption and scattering of the laser light in the volume probed by the pulses with no change in the wavelength, which contrasts with inelastic methods like Raman lidar.
- The lidar return-signals consist of a series of pulses scattered back to the lidar and are received over a range determined by the transmitter–receiver geometry, see Fig. 4.
- As described below, the signal originates from two-way attenuated backscattering by the atmospheric constituents.
- We refer here to several specialized monographs available on the general theory of lidar [12, 13, 53].

General Backscatter Lidar Arrangement

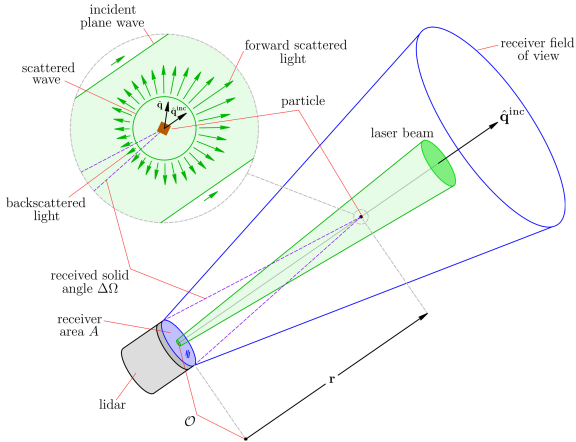

A pulsed laser beam is emitted from the lidar transmitter, illuminating a column of the atmosphere. When a pulse reaches an aerosol particle at range **r**, it scatters in all directions. The lidar return signal is the portion of light backscattered to the receiver's area A, defining the received solid angle $\Delta\Omega = A\,r^{-2}$. The exact backscattering direction is $-\hat{\mathbf{q}}^{\text{inc}}$.

Elastic Lidar Equation under SSA

- The elastic lidar equation under the single-scattering approximation (SSA) assumes that the incident wave is scattered only once, ignoring multiple-scattering events.
- SSA is never exactly satisfied but often involves little error in practical applications.
- Example : Mishchenko's superposition T-matrix method shows negligible error for particle collections with specific conditions [16] :
  - Average particle-to-particle separation $\langle d \rangle$ with $k\langle d \rangle > 30$
  - Particle packing-density less than 1%
- Such conditions are often present in lidar applications.

Elastic Lidar Equation under SSA (cont.)

- Under the single-scattering approximation, the lidar equation can be derived from the Radiative Transfer Equation (RTE) for an ensemble of particles [54] :

$$\hat{\mathbf{q}} \cdot \nabla \widetilde{\mathbf{I}}(\mathbf{r}, \hat{\mathbf{q}}) = \underbrace{-n_{\mathrm{o}}(\mathbf{r}) \langle \mathbf{K}(\hat{\mathbf{q}}) \rangle \cdot \widetilde{\mathbf{I}}(\mathbf{r}, \hat{\mathbf{q}})}_{\text{extinction term}} + \underbrace{n_{\mathrm{o}}(\mathbf{r}) \int_{4\pi} \mathrm{d}\hat{\mathbf{q}}' \left\langle \mathbf{Z}\left(\hat{\mathbf{q}}, \hat{\mathbf{q}}'\right) \right\rangle \cdot \widetilde{\mathbf{I}}(\mathbf{r}, \hat{\mathbf{q}}')}_{\text{scattering term}} . \qquad (1)$$

- ▷ $\mathbf{r} = r\hat{\mathbf{r}}$: distance vector ; $\hat{\mathbf{q}}$: propagation unit vector
- ▷ $n_{\mathrm{o}}(\mathbf{r})$: local particle number density at $\mathbf{r}$ (units : inverse volume)
- ▷ $\widetilde{\mathbf{I}}(\mathbf{r}, \hat{\mathbf{q}})$: specific intensity, 4×1 column vector (units : radiance [$\mathrm{W\,m^{-2}\,sr^{-1}}$])
- ▷ $\mathbf{K}(\hat{\mathbf{q}})$: the 4×4 Stokes extinction matrix with units of area
- ▷ $\mathbf{Z}(\hat{\mathbf{q}}, \hat{\mathbf{q}}')$: the 4×4 Stokes phase matrix with units of area per solid angle.

Elastic Lidar Equation under SSA (cont.)

- The first term, or the extinction term, on the right-hand side of Eq. (1) describes the change of specific intensity caused by extinction
- The second term, or the scattering term, describes the contribution of light illuminating a small volume element from all directions $\hat{\mathbf{q}}'$ and scattered in the direction $\hat{\mathbf{q}}$.
- In deriving the lidar equation below, we neglect thermal emission from the atmospheric constituents and assume that the only light reaching the lidar receiver is that backscattered by the scattering medium.
- Background radiance from the atmosphere is neglected in the following for the sake of simplicity.

Step 1 : Attenuated Forward Specific Intensity

- First, let us calculate the attenuated *forward* specific intensity using the extinction term in the RTE.
- The attenuated specific intensity along the path between the transmitter, which is located at the origin $\mathbf{r} = \boldsymbol{\mathcal{O}}$ in Fig. 4, and the scattering medium, located at $\mathbf{r}$, is thus,

$$\hat{\mathbf{q}} \cdot \nabla \widetilde{\mathbf{I}}(\mathbf{r}, \hat{\mathbf{q}}) = -n_0(\mathbf{r}) \langle \mathbf{K}(\hat{\mathbf{q}}) \rangle \cdot \widetilde{\mathbf{I}}(\mathbf{r}, \hat{\mathbf{q}}). \tag{2}$$

- The Stokes extinction matrix can be simplified as a diagonal matrix with elements equal to the average extinction cross-section per particle $\langle C^{\text{ext}} \rangle$ under the assumption of a macroscopically isotropic and symmetric scattering medium.

$$\langle \mathbf{K}(\hat{\mathbf{q}}) \rangle = \langle C^{\text{ext}} \rangle \mathbb{I}, \tag{3}$$

Where $\mathbb{I}$ represents the 4×4 identity matrix.

Step 1 : Attenuated Forward Specific Intensity (cont.)

- Equation (2) can be integrated over the forward path, i.e. from the transmitter at $\mathcal{O}$ to the scattering medium at $\mathbf{r}$, to give the attenuated *forward* specific intensity $\widetilde{\mathbf{I}}^{\text{for}}$ as,

$$\widetilde{\mathbf{I}}^{\text{for}}(\mathbf{r}, \hat{\mathbf{q}}) = \widetilde{\mathbf{I}}^{\text{inc}} \exp\left(- \int_0^r n_{\text{o}}(\mathbf{r}') \left\langle C^{\text{ext}}(\mathbf{r}') \right\rangle \mathrm{d}\mathbf{r}' \right), \tag{4}$$

- Where $\widetilde{\mathbf{I}}^{\text{inc}}$ is the specific intensity of the emitted laser pulses and the notation $\langle C^{\text{ext}}(\mathbf{r}) \rangle$ denotes the possibility that the average extinction per particle may be range dependent.

Step 2 : Scattered Specific Intensity

- Second, we calculate the *scattered* specific intensity using the scattering term. The attenuated forward specific intensity $\widetilde{\mathbf{I}}^{\text{for}}$ is scattered by the scattering medium in the backscattering direction $-\hat{\mathbf{q}}^{\text{inc}}$.
- Invoking the SSA, only a single scattering event is considered and the second term of the RTE, Eq. (1), is simplified to :

$$\hat{\mathbf{q}} \cdot \nabla \widetilde{\mathbf{I}}(\mathbf{r}, \hat{\mathbf{q}}) = n_{\text{o}}(\mathbf{r}) \int_{\hat{\mathbf{q}}=-\hat{\mathbf{q}}^{\text{inc}}} \mathrm{d}\hat{\mathbf{q}}' \left\langle \mathbf{Z}\left(\hat{\mathbf{q}}', \hat{\mathbf{q}}\right) \right\rangle \cdot \widetilde{\mathbf{I}}^{\text{for}}(\mathbf{r}, \hat{\mathbf{q}}'). \tag{5}$$

- The integration in Eq. (5) is over differential solid angle in the backward direction, and so, we get $\mathbf{I}^{\text{for}}$, which is the 4×1 Stokes vector,

$$\hat{\mathbf{q}} \cdot \nabla \widetilde{\mathbf{I}}(\mathbf{r}, \hat{\mathbf{q}}) = n_{\text{o}}(\mathbf{r}) \left\langle \mathbf{Z}\left(-\hat{\mathbf{q}}^{\text{inc}}, \hat{\mathbf{q}}^{\text{inc}}\right) \right\rangle \cdot \mathbf{I}^{\text{for}}(-\hat{\mathbf{q}}^{\text{inc}}). \tag{6}$$

Step 2 : Scattered Specific Intensity

- If the number density of particles remains constant within the volume probed by the laser with pulse duration τ, then $n_o(\mathbf{r}) = n_o$, and the specific scattered intensity $\widetilde{\mathbf{I}}^{\text{sca}}$ can be found from Eq. (6) as,

$$\widetilde{\mathbf{I}}^{\text{sca}}(\mathbf{r}, -\hat{\mathbf{q}}^{\text{inc}}) = n_o \left\langle \mathbf{Z}\left(-\hat{\mathbf{q}}^{\text{inc}}, \hat{\mathbf{q}}^{\text{inc}}\right)\right\rangle \cdot \int_{-c\tau/4}^{c\tau/4} \mathrm{d}\mathbf{r}' \cdot \mathbf{I}^{\text{for}}(\mathbf{r}, \hat{\mathbf{q}}). \tag{7}$$

- The integration in Eq. (7) is carried out over the volume of the laser pulse at range $\mathbf{r}$ giving :

$$\widetilde{\mathbf{I}}^{\text{sca}}(\mathbf{r}, -\hat{\mathbf{q}}^{\text{inc}}) = \frac{c\tau}{2}\, n_o \left\langle \mathbf{Z}\left(-\hat{\mathbf{q}}^{\text{inc}}, \hat{\mathbf{q}}^{\text{inc}}\right)\right\rangle \cdot \mathbf{I}^{\text{for}}(\mathbf{r}, -\hat{\mathbf{q}}^{\text{inc}}). \tag{8}$$

Step 3 : Backscattered Specific Intensity

- Lastly, we calculate the *backscattered* specific intensity using the extinction term of the RTE.
- The attenuated specific intensity along the path between the scattering medium and the receiver, which again is located at the origin $\mathbf{r} = \mathcal{O}$ in Fig. 4, is thus,

$$\widetilde{\mathbf{I}}^{\mathrm{bac}}(\mathbf{r}, -\hat{\mathbf{q}}^{\mathrm{inc}}) = \widetilde{\mathbf{I}}^{\mathrm{sca}}(\mathbf{r}, -\hat{\mathbf{q}}^{\mathrm{inc}}) \exp\left(-n_{\mathrm{o}} \int_0^r \langle C^{\mathrm{ext}}(\mathbf{r}') \rangle \, \mathrm{d}\mathbf{r}' \right), \tag{9}$$

- Or after using Eq. (4), Eq. (8), and Eq. (9) we get

$$\widetilde{\mathbf{I}}^{\mathrm{bac}}(\mathbf{r}, -\hat{\mathbf{q}}^{\mathrm{inc}}) = \frac{c\tau}{2} \, n_{\mathrm{o}} \left\langle \mathbf{Z}\left(-\hat{\mathbf{q}}^{\mathrm{inc}}, \hat{\mathbf{q}}^{\mathrm{inc}}\right) \right\rangle \cdot \mathbf{I}^{\mathrm{inc}}(\mathbf{r}, \hat{\mathbf{q}}^{\mathrm{inc}}) \exp\left(-2\, n_{\mathrm{o}} \int_0^r \langle C^{\mathrm{ext}}(\mathbf{r}') \rangle \, \mathrm{d}\mathbf{r}' \right). \tag{10}$$

Attenuated Backscattering Stokes Matrix

Let us now define the attenuated backscattering Stokes matrix $\mathbf{U}(\mathbf{r})$ as,

$$\mathbf{U}(\mathbf{r}) = n_o \left\langle \mathbf{Z}\left(\hat{\mathbf{q}}^{\text{inc}}, -\hat{\mathbf{q}}^{\text{inc}}\right)\right\rangle \exp\left(-2\, n_o \int_0^r \left\langle C^{\text{ext}}\left(\mathbf{r}'\right)\right\rangle \mathrm{d}\mathbf{r}'\right) \tag{11}$$

and thus, the backward specific intensity can be written as,

$$\widetilde{\mathbf{I}}^{\text{bac}}(\mathbf{r}, -\hat{\mathbf{q}}^{\text{inc}}) = \frac{c\tau}{2}\, \mathbf{U}(\mathbf{r}) \cdot \widetilde{\mathbf{I}}^{\text{inc}}(\mathbf{r}, \hat{\mathbf{q}}^{\text{inc}}). \tag{12}$$

Backscattered Power Calculation

- The backscattered power $\mathbf{P}^{\text{bac}}$, defined as a 4×1 column vector with units of power [W] for each component, is calculated from $\widetilde{\mathbf{I}}^{\text{bac}}$ in Eq. (12) for a given range $\mathbf{r}$ and for a solid angle $\Delta\Omega = Ar^{-2}$ subtended by the receiver area A with respect to the direction $-\hat{\mathbf{q}}^{\text{inc}}$ as,

$$\mathbf{P}^{\text{bac}}(\mathbf{r}, -\hat{\mathbf{q}}^{\text{inc}}) = A\Delta\Omega\widetilde{\mathbf{I}}^{\text{bac}}(\mathbf{r}, -\hat{\mathbf{q}}^{\text{inc}}), \tag{13}$$

- Simplifying further, we get :

$$\mathbf{P}^{\text{bac}}(\mathbf{r}, -\hat{\mathbf{q}}^{\text{inc}}) = A^2 \frac{c\tau}{2} \mathbf{U}(\mathbf{r}) \cdot \widetilde{\mathbf{I}}^{\text{inc}}(\mathbf{r}, \hat{\mathbf{q}}^{\text{inc}})\, r^{-2}. \tag{14}$$

Elastic Lidar Equation

Equation 14 is the *elastic lidar equation* derived from the RTE under the single-scattering and full-overlap approximations. This equation is often found in the following scalar form [12, 13] where $\mathrm{O}(\mathbf{r})$ is the overlap function, which represents the coupling efficiency between the lidar emitter and receiver :

$$\mathrm{P}(r) = \mathrm{K_o}\, \mathrm{O}(r)\, \mathrm{U}(r)\, r^{-2}. \tag{15}$$

where $\mathrm{K_o}$ is the radiometric lidar constant with units of power times cubic meter times solid angle [$\mathrm{W\,m^3\,sr}$], which depends either on the transmitted laser pulse-intensity $\mathrm{I_o}$, pulse-power $\mathrm{P_o}$, or pulse-energy energy $\mathcal{E}_\mathrm{o}$, as

$$\mathrm{K_o} = \mathrm{I_o}\, \frac{c\tau}{2} A^2 = \mathrm{P_o}\, \frac{c\tau}{2} A = \mathcal{E}_\mathrm{o}\, \frac{c}{2} A. \tag{16}$$

Elastic Lidar Equation

In this scalar form, only the first element of the Stokes phase matrix is considered, i.e.,

$$\frac{\mathrm{d}\langle C^{\mathrm{bac}}\rangle}{\mathrm{d}\Omega}(r) = \left\langle Z_{11}\left(\hat{\mathbf{q}}^{\mathrm{inc}}, -\hat{\mathbf{q}}^{\mathrm{inc}}; r\right)\right\rangle . \tag{17}$$

Thus, Eq. (11) can be simplified as a scalar function, referred to here as the attenuated backscatter function $\mathrm{U}(r)$:

$$\mathrm{U}(r) = \beta(r)\exp\left(-2\int_0^r \alpha(r')\,\mathrm{d}r'\right), \tag{18}$$

where $\alpha(r)$ and $\beta(r)$ are, respectively, the range-dependent scalar *volume* extinction and backscattering coefficients defined as,

$$\alpha(r) = n_{\mathrm{o}}\langle C^{\mathrm{ext}}(r)\rangle \quad \text{and} \quad \beta(r) = n_{\mathrm{o}}\frac{\mathrm{d}\langle C^{\mathrm{bac}}\rangle}{\mathrm{d}\Omega}(r). \tag{19}$$

Lidar Ratio (LR)

- The under-determined nature of the lidar problem, i.e., the retrieval of two unknown parameters from only one lidar measurement, appears in Eq. (15) via Eqs. (18)-(65) where α and β are the unknowns. The inversion of this ill-posed problem requires an intrinsic relationship between backscattering and extinction cross-sections, namely the lidar extinction-to-backscatter ratio or simply the Lidar Ratio $\mathrm{LR}(r)$. A common practice is to assume that these two cross-sections are related as [55, 56, 57]

$$\mathrm{LR}(r) = \frac{\alpha(r)}{\beta(r)} = \langle C^{\mathrm{ext}}(r) \rangle \left[\frac{\mathrm{d}\langle C^{\mathrm{bac}} \rangle}{\mathrm{d}\Omega}(r) \right]^{-1}. \tag{20}$$

- The LR strongly depends on the particle properties and can be established from extensive lidar campaigns [58, 59] or from light-scattering models accounting for irregularly shaped-particles [60, 17, 61, 18].

3. Extinction of aerosols

Extinction - Definitions

Extinction refers to the attenuation of light by particles due to absorption and scattering, quantified by the extinction cross section C^{ext} [62, 63]. For a nonmagnetic spherical particle of radius R and complex refractive index $m = n + \kappa i$ in vacuum, illuminated by a linearly polarized plane wave, the electric and magnetic fields are :

$$\mathbf{E}^{\text{inc}}(\mathbf{r}) = \mathbf{E}_0^{\text{inc}} \exp(ikr\hat{\mathbf{r}} \cdot \hat{\mathbf{n}}^{\text{inc}}), \quad \mathbf{B}^{\text{inc}}(\mathbf{r}) = \frac{k}{\omega}\hat{\mathbf{n}}^{\text{inc}} \times \mathbf{E}^{\text{inc}}(\mathbf{r}). \tag{21}$$

$\mathbf{E}_0^{\text{inc}}$ is the amplitude and polarization of the incident electric field and $\hat{\mathbf{n}}^{\text{inc}}$ is the propagation direction. All field quantities are time-harmonic with the factor $\exp(-i\omega t)$, where $\omega = kc$ and c is the speed of light. This time factor will be suppressed for brevity.

Extinction - Definitions

- Let the surface and interior volume of the particle be $\mathcal{S}$ and V^{int}, respectively.
- The particle is centered at the origin and enclosed by an imaginary spherical surface $\mathcal{S}^{\text{en}}$ of radius R_{en} and normal $\hat{\mathbf{n}}_{\text{en}}$, see Fig. 1.
- The volume bounded by $\mathcal{S}^{\text{en}}$, excluding V^{int}, will be called the external volume V^{ext}.

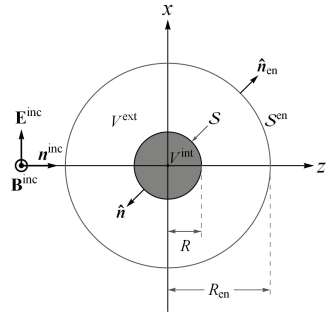

Figure – Arrangement used to derive the extinction cross section for a spherical particle.

Extinction - Definitions

The total wave that exists when the particle is present is then artificially decomposed into the superposition of the original incident wave and a modification, called the scattered wave, i.e.,

$$\mathbf{E}(\mathbf{r}) = \mathbf{E}^{\text{inc}}(\mathbf{r}) + \mathbf{E}^{\text{sca}}(\mathbf{r}), \quad \mathbf{B}(\mathbf{r}) = \mathbf{B}^{\text{inc}}(\mathbf{r}) + \mathbf{B}^{\text{sca}}(\mathbf{r}). \tag{22}$$

Extinction - Definitions

Sensors in light scattering measurements respond only to the component of the time-average of the electromagnetic energy flow **S** that is directed into their sensitive part.

If the sensor resides in the forward direction looking at the oncoming incident and scattered waves, **S** is determined by the *total* wave.

Extinction - Definitions

This energy flow is given by the Poynting vector [62, 64] :

$$\langle \mathbf{S}(\mathbf{r}) \rangle_t = \frac{1}{2\mu_o} \mathrm{Re}\{ \mathbf{E}(\mathbf{r}) \times [\mathbf{B}(\mathbf{r})]^* \} = \langle \mathbf{S}^{\mathrm{inc}}(\mathbf{r}) \rangle_t + \langle \mathbf{S}^{\mathrm{sca}}(\mathbf{r}) \rangle_t + \langle \mathbf{S}^{\mathrm{ext}}(\mathbf{r}) \rangle_t, \tag{23}$$

where $\langle \ldots \rangle_t$ denotes time-averaging. In Eq. (23), μ_o is the permeability of free space, $[\ldots]^*$ represents complex conjugation, $\langle \mathbf{S}^{\mathrm{inc}} \rangle_t$ involves only the incident fields, $\langle \mathbf{S}^{\mathrm{sca}} \rangle_t$ involves only the scattered fields, and $\langle \mathbf{S}^{\mathrm{ext}} \rangle_t$ involves the product of the incident and scattered fields i.e.,

$$\langle \mathbf{S}^{\mathrm{ext}} \rangle_t = \frac{1}{2\mu_o} \mathrm{Re}\Big\{ \mathbf{E}^{\mathrm{inc}}(\mathbf{r}) \times \big[\mathbf{B}^{\mathrm{sca}}(\mathbf{r})\big]^* + \mathbf{E}^{\mathrm{sca}}(\mathbf{r}) \times \big[\mathbf{B}^{\mathrm{inc}}(\mathbf{r})\big]^* \Big\}. \tag{24}$$

Extinction - Definitions

The extinction cross section C^{ext} is obtained by integrating the part of Eq. (24) that flows into $\mathcal{S}^{\text{en}}$,

$$C^{\text{ext}} = -\frac{1}{I^{\text{inc}}} \oint_{\mathcal{S}^{\text{en}}} \langle \mathbf{S}^{\text{ext}}(\mathbf{r}) \rangle_t \cdot \hat{\mathbf{r}} \, \mathrm{d}S, \tag{25}$$

where $I^{\text{inc}} = (1/2)\sqrt{\epsilon_o/\mu_o}|\mathbf{E}_0^{\text{inc}}|^2$ is the intensity of the incident wave and ϵ_0 is the permittivity of free space. Similarly, the scattering and absorption cross sections C^{sca} and C^{abs} are given by the integration of $\langle \mathbf{S}^{\text{sca}} \rangle_t$ and $\langle \mathbf{S} \rangle_t$ over $\mathcal{S}^{\text{en}}$, respectively as shown in [64].

Extinction - Definitions

Poynting's theorem shows that extinction expresses the conservation of energy in any *elastic* scattering situation as

$$C^{\text{ext}} = C^{\text{abs}} + C^{\text{sca}}. \tag{26}$$

The cross sections, C^{abs} and C^{sca}, in Eq. (26) stem from energy flows that represent losses to the energy contained $\mathcal{S}^{\text{en}}$. Absorption converts energy to other forms (thermal etc.) thus acting as a sink, and scattering carries energy away through $\mathcal{S}^{\text{en}}$, again acting as a sink. Extinction is often, but not always, associated with an attenuation of the incident beam along its propagation direction [65]. One will see below how interference between the incident and scattered waves is an integral part of the redistribution of energy in the extinction process.

Extinction - Definitions

Notice that Eq. (25) yields C^{ext} in terms of the scattered fields on $\mathcal{S}^{\text{en}}$, and is valid at *any* distance from the particle. However, it is more common to expand $\mathcal{S}^{\text{en}}$ to infinity and use the *optical theorem* to find C^{ext} in a simple manner as [64]

$$C^{\text{ext}} = \frac{4\pi}{k|\mathbf{E}_{\text{o}}^{\text{inc}}|^2} \text{Im}\left\{ \mathbf{E}_1^{\text{sca}}(\hat{\mathbf{n}}^{\text{inc}}) \cdot \left[\mathbf{E}_{\text{o}}^{\text{inc}}\right]^* \right\} \tag{27}$$

where $\mathbf{E}_1^{\text{sca}}$ is the scattering amplitude, defined by

$$\mathbf{E}^{\text{sca}}(\mathbf{r}) = \frac{\exp(ikr)}{r} \mathbf{E}_1^{\text{sca}}(\hat{\mathbf{r}}), \quad kr \to \infty. \tag{28}$$

Extinction - Definitions

From Mie theory [66, 63], C^{ext} for a spherical particle can be written as an infinite series of Mie coefficients a_n and b_n [63] as :

$$C^{\text{ext}} = \frac{2\pi}{k^2} \sum_{n=0}^{\infty} (2n+1) \text{Re}\left\{a_n + b_n\right\}. \tag{29}$$

The extinction efficiency factor Q^{ext} is defined from the geometrical cross-section C^{geo} as

$$Q^{\text{ext}} = \frac{C^{\text{ext}}}{C^{\text{geo}}}. \tag{30}$$

The meaning of Q^{ext} is the amount of power removed from the region bounded by $\mathcal{S}^{\text{en}}$, due to scattering and absorption, relative to the amount of power contained in the portion of the incident wave geometrically intercepted by the particle [63].

Volume Extinction Coefficient

In lidar analysis, the extinction cross section C^{ext} or efficiency Q^{ext} should always be integrated over the aerosol size distribution $n(R)$ to calculate the range-dependent volume extinction coefficient α^{aer} defined as

$$\alpha^{\text{aer}}(r) = \int_{R_{\text{min}}}^{R_{\text{max}}} n(r, R)\, C^{\text{ext}}(r, R)\, \mathrm{d}R. \tag{31}$$

Here, we assume the SSA and that the aerosol is adequately represented as an isotropic scattering medium formed by an ensemble of particles of size R spanning a minimum and maximum particle-size R_{min} and R_{max}, respectively.

Measurements of Extinction

Distinct methods alllow the measurement of the extinction cross-sections of aerosols

Each method has its advantages and disadvantages, which will be explained. These methods are typically used in laboratory settings although some work has extended them to the field. Laboratory measurements of specific classes of particles, such as smoke soot and mineral dust, can be helpful in lidar contexts as they can provide estimates for the extinction component of the lidar ratio (LR).

In the following, two methods will be detailed :

1. Small-Angle Light-Scattering (SALS)
2. Digital Holography (DH)

Measurements of Extinction - Small-Angle Light-Scattering

- Over decades, many elastic light-scattering devices have been developed to measure light-scattering patterns from individual aerosol particles [67, 68, 69, 70, 71, 72].
- Scattering close to the forward direction, i.e., small angle scattering, is especially useful for particle sizing. Such measurements are challenging because in many situations the majority of light incident on a particle is unscattered and will thus dominate the weak scattered light at a detector viewing small scattering angles.
- One approach to separate intense unscattered light from near-forward scattered light involves a lens that removes much of the unscattered light by use of a spatial filter in the Fourier plane of the lens [73, 74, 75, 76].

Measurements of Extinction - Small-Angle Light-Scattering

- Let us explore a simple experiment developed in [77] to measure the two-dimensional small angle light scattering (2D-SALS) pattern around the forward direction for single particles fixed to a glass stage.
- This experiment is based on the spatial-filtering concept in [75], but with the refractive optical elements replaced by curved mirrors. The term 2D here refers to the two scattering angles θ and ϕ.
- Individual particles are deposited on an anti-reflection coated window (S). The right-most inset shows a particle on S, the z-axis, and the scattering angle θ. Unscattered light is shown with solid lines while scattered light is in dashed lines. Scattered and unscattered light are separated by the off-axis parabolic (OAP) mirror, which features a 3 mm diameter through-hole. Scattered light is then relayed by a second OAP to the IR-CCD sensor. The left-most inset shows a typical 2D-SALS pattern in false color.

Measurements of Extinction - Small-Angle Light-Scattering

Arrangement to measure 2D-SALS patterns from single microparticles with white light emited by a supercontinuum laser [77].

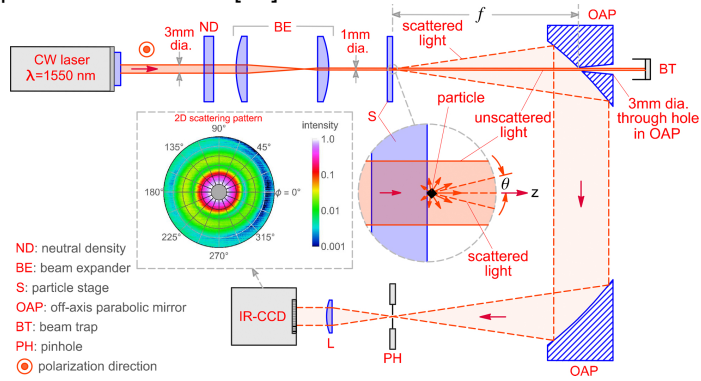

Measurements of Extinction - Small-Angle Light-Scattering

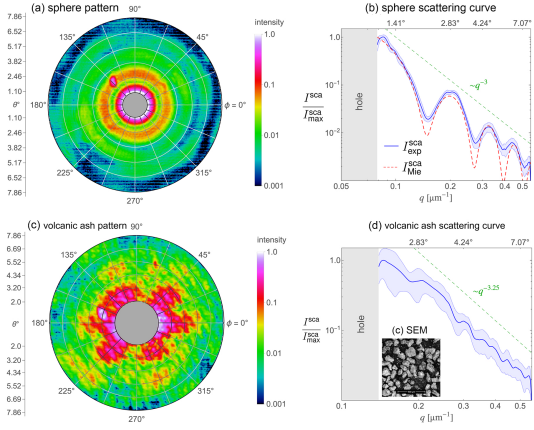

Measurements of Extinction - Small-Angle Light-Scattering

- Measured 2D-SALS patterns and scattering curves for a 50 µm diameter polyethylene microsphere and a single volcanic ash particle from the Popocatépetl volcano [77].
- The measured 2D-SALS pattern is shown in (a) in false color in log scale.
- The azimuthal average of this pattern, i.e., the scattering curve $I^{\text{sca}}_{\text{exp}}$, is plotted as a function of q in log-log scale in (b) as the blue curve.
- The blue shaded region in (b) shows the azimuthal variation of the 2D pattern.
- Also in (b) is a comparison to Mie theory, $I^{\text{sca}}_{\text{Mie}}$, plotted in red dash for a sphere with $D = 2R = 50.66$ µm and $m = 1.43 + 0.0245i$.
- Plots (c) and (d) show the same for the volcanic ash particle, except a comparison to a theoretical curve is not possible in (d) as the particle properties are unknown.
- The notation $I^{\text{sca}}/I^{\text{sca}}_{\text{max}}$ refers to the curves being normalized to the maximum of the measured scattered intensity.

Measurements of Extinction - Digital Holography

- Digital holography (DH) is a powerful method to characterize coarse aerosol particles, providing size and shape information without inversion, e.g., see [78, 76].
- The method can also measure a particle's extinction cross section C^{ext} [79, 80].
- DIH uses a 2D sensor (CCD or CMOS) to view an expanded, collimated laser beam.

Principle of operation :

- First, a reference measurement $I^{\text{ref}}(x, y)$ is taken without particles.
- Then, a particle is introduced, and the sensor captures the hologram $I^{\text{holo}}(x, y)$, where the incident and scattered waves interfere.
- The contrast hologram $I^{\text{con}}(x, y) = I^{\text{ref}}(x, y) - I^{\text{holo}}(x, y)$ is then processed using the Fresnel-Kirchhoff diffraction integral to generate a silhouette-like image of the particle.

Measurements of Extinction - Digital Holography

Extinction is described as a loss of radiant energy flow in a beam due to a particle absorbing and scattering the light. It is as if the particle casts a shadow along the beam axis. The only way to remove a wave, or a portion of a wave, from a region of space is for an interference process to redistribute the undisturbed wave [81].

Extinction can also be viewed as an interference process between the incident and scattered waves. As shown in [80], C^{ext} is measured as the difference of the net response of a two-dimensional sensor looking into the incident wave when a particle is not present and when it is present in the wave [79, 65, 82].

Measurements of Extinction - Digital Holography

Let us define

$$I_{\mathrm{o}}^{\mathrm{sen}}(\theta) = \frac{1}{I^{\mathrm{inc}}} \int_{\mathcal{S}_2} \langle \mathbf{S}^{\mathrm{inc}} \rangle_t \cdot \hat{\mathbf{z}} \, \mathrm{d}a \quad \text{and} \quad I^{\mathrm{sen}}(\theta) = \frac{1}{I^{\mathrm{inc}}} \int_{\mathcal{S}_2} \langle \mathbf{S} \rangle_t \cdot \hat{\mathbf{z}} \, \mathrm{d}a. \tag{32}$$

where $I_{\mathrm{o}}^{\mathrm{sen}}$ and I^{sen} are the normalized total sensor-response without and with the particle. The response is the power received by the sensor due to the energy flow $\langle \mathbf{S}^{\mathrm{inc}} \rangle_t$ or $\langle \mathbf{S} \rangle_t$ integrated across $\mathcal{S}_2$, subtending a solid angle θ_{sen}.

Measurements of Extinction - Digital Holography

The difference between these measurements is

$$
\begin{aligned}
f(\theta) &= I_{\mathrm{o}}^{\mathrm{sen}}(\theta) - I^{\mathrm{sen}}(\theta) \\
&= \frac{1}{I^{\mathrm{inc}}}\Big[\underbrace{\int_{\mathcal{S}_1} \langle \mathbf{S}^{\mathrm{sca}} \rangle_t \cdot \hat{\mathbf{n}}\, \mathrm{d}a}_{I_1} - W^{\mathrm{sca}} + \underbrace{\int_{\mathcal{S}_1} \langle \mathbf{S}^{\mathrm{ext}} \rangle_t \cdot \hat{\mathbf{n}}\, \mathrm{d}a}_{I_2} + W^{\mathrm{ext}}\Big].
\end{aligned}
\tag{33}
$$

To understand the meaning of Eq. (33), realize that if $\theta \ll 1$, $\mathcal{S}_2$ is small and $\mathcal{S}_1$ is almost a closed surface. Then, I_1 is nearly equal to W^{sca}, which is canceled by the second term in Eq. (33). We also see that I_2 is nearly equal to $-W^{\mathrm{ext}}$ as explained in [65], which is canceled by the last term in Eq. (33). In all then, when θ is small, we find that $f \simeq 0$.

Measuring Extinction with Digital Holography

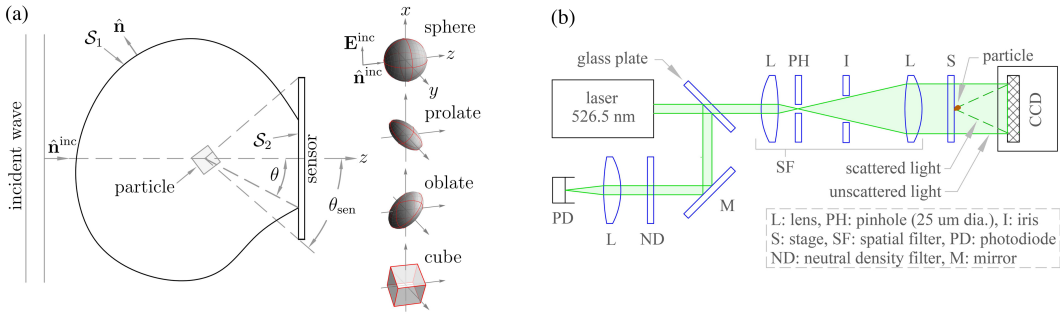

Figure – Measuring extinction with digital holography. In (a) are sketches of the surfaces $\mathcal{S}_1$ and $\mathcal{S}_2$ in addition to the associated θ and θ_{sen} needed to derive Eqs. (32)-(??). Note that $\mathcal{S}_2$ is a surface covering a variable portion of the sensor.

Measuring Extinction with Digital Holography

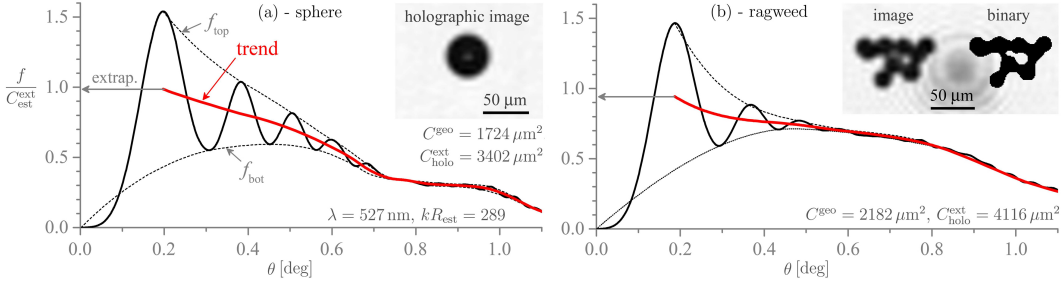

Figure – Estimation of extinction cross sections from digital hologram measurements. Shown here are the $f(\theta)$ curves of Eq. (33) obtained by integrating measured contrast holograms I^{con} for a 50 µm diameter glass sphere, in (a), and a ragweed-pollen cluster in (b) [80]. Hologram-derived images of these particles are shown inset by applying the Fresnel-Kirchhoff diffraction integral to I^{con}.

4. Backscattering of aerosols

Backscattering - Definitions

The primary observable is the differential backscattering cross-section $\mathrm{d}C^{\mathrm{bac}}/\mathrm{d}\Omega$. This quantity is simply Eq. (**??**) evaluated in the exact backward direction $\hat{\mathbf{n}}^{\mathrm{bac}} = -\hat{\mathbf{n}}^{\mathrm{inc}}$, i.e.,

$$\frac{\mathrm{d}C^{\mathrm{bac}}}{\mathrm{d}\Omega} = \frac{\mathrm{d}C^{\mathrm{sca}}}{d\Omega}(\hat{\mathbf{n}}^{\mathrm{bac}}) = \frac{r^2}{I^{\mathrm{inc}}} \left| \langle \mathbf{S}^{\mathrm{sca}}(r\hat{\mathbf{n}}^{\mathrm{bac}}) \rangle_t \cdot \hat{\mathbf{n}}^{\mathrm{bac}} \right|. \tag{34}$$

This quantity is commonly used in lidar and has the units of area per unit of solid angle, $[\mathrm{m}^2/\Omega]$. For spherical particles specifically, Mie theory gives the differential backscattering cross-section in terms of the amplitude scattering matrix S or as an infinite series of the Mie coefficients a_n and b_n as [63]

Backscattering - Definitions

$$\frac{\mathrm{d}C^{\mathrm{bac}}}{\mathrm{d}\Omega} = \frac{1}{k^2}\left|S_1(\pi)\right|^2 = \frac{1}{2k^2}\sum_{n=0}^{\infty}(-1)^n(2n+1)(a_n - b_n). \tag{35}$$

The backscattering cross-section C^{bac} is defined in [83] as an equivalent surface with units of area [m^2]. It can be seen as the scattering cross-section of an hypothetical particle that scatters the incident wave isotropically as

$$C^{\mathrm{bac}} = 4\pi\frac{\mathrm{d}C^{\mathrm{bac}}}{\mathrm{d}\Omega} = \frac{4\pi}{k^2}\left|S_1(\pi)\right|^2, \tag{36}$$

where 4π denotes steradian, i.e., all directions. An especially important quantity derived from Eq. (36) is the backscattering efficiency Q^{bac} defined in analogy to Eq. (30) as

$$Q^{\mathrm{bac}} = \frac{C^{\mathrm{bac}}}{C^{\mathrm{geo}}}. \tag{37}$$

Volume Backscattering Coefficient

Finally, we note that the quantities in Eq. (34) and Eqs. (36)-(37) should always be integrated over the particle size distribution when dealing with atmospheric aerosols to properly calculate the volume backscattering coefficient β^{aer}, which is then given by

$$\beta^{\text{aer}}(r) = \int_{R_{\min}}^{R_{\max}} n(r, R) \frac{\mathrm{d}C^{\text{bac}}}{\mathrm{d}\Omega}(r, R)\, \mathrm{d}R, \tag{38}$$

where $n(R)$ is the particle size distribution of an isotropic scattering medium formed by an ensemble of particles of radius R.

Measurements of Backscattering

- Numerous studies have reported light-scattering measurements for various aerosols, but most do not consider exact backward scattering due to weak signals and instrumentation limits [67, 68, 69, 70, 71, 72, 73, 74].
- Available data may be extrapolated. Methods like microwave analog and optical tweezers have achieved limited backward scattering measurements [84, 85, 86, 87, 88] to isolate single aerosol particles where light-scattering measurements have been achieved.
- Only a limited number of publications have reported backscattering measurements by single particles in the exact backward direction. Notable works include Sassen [89], Szymanski et al. [90], Sakai et al. [91], and Miffre et al. [92, 93].

Measurements of Backscattering

- Whereas the extinction cross-section is governed by diffraction and depends on the particle size and shape, the backscattering cross-section is more sensitive to the morphology and surface roughness. Fu et al. [94] and Pan et al. [95] measure the backscattering patterns of single optically-trapped particles and examine different particle sizes, shape, and surface roughness.
- Two-dimensional backscattering patterns show concentric rings for spherical particles, while irregular shapes exhibit less symmetry. Backscattering is highly sensitive to particle morphology and surface structure.
- New methods and apparatus are needed to improve lidar ratio determinations and validate models.

Measurements of Backscattering - Backscattering Small-Angle L

Few methods have been developed to measure accurately the backscattering cross-sections of aerosols in laboratory.

In the following, a novel method named Backscattering Small-Angle Light-Scattering (B-SALS) is presented.

4. Lidar inverse methods

Lidar inversion

- Various methods and techniques for lidar-signal inversion are based on Bernoulli's differential equation form of the lidar equation [96, 97, 98, 99, 55, 56, 100, 101].
- The slope method retrieves the extinction coefficient of homogeneous atmospheres by assuming constant backscattering and extinction coefficients [97, 99].
- Advanced methods, such as boundary point methods, apply to inhomogeneous atmospheres :
  - Fernald et al. [55] present a forward inverse-method for backscatter profiles.
  - Klett et al. [56] propose a more stable backward method for a one-component atmospheric model.
  - Fernald et al. [57] and Sasano et al. [100] improve the method with a two-component atmospheric model.
- These methods are often referred to as the Klett-Fernald-Sasano method.

Lidar inversion - Challenges

- Inversion methods for elastic lidar require accurate lidar extinction-to-backscatter ratio [57, 56].
- This ratio depends on aerosol particle properties and is crucial for aerosol classification.
- Incorrect assumptions of this ratio can lead to significant errors in lidar retrievals [100, 102].
- Advanced techniques like High Spectral Resolution Lidar and Raman Lidar measure extinction and backscatter profiles directly [103, 104, 105, 106, 107].
- These techniques are sensitive to background noise and are better suited for clean atmospheres or space applications.
- Ongoing research and numerous lidar campaigns aim to improve the assessment of the extinction-to-backscatter ratio.

Lidar inversion - Slope method

The basis lies in finding an operator that linearizes the lidar equation (Kunz and Leeuw). The logarithm of the range corrected lidar signal gives

$$\ln(\mathrm{RCS}(r)) = \ln(K_o) + \ln(O(r)) + \ln(\beta(r)) - 2\int_0^r \alpha(r')dr' \tag{39}$$

where $RCS(r)$ is the range-corrected signal defined as :

$$RCS(r) = P(r)r^2 \tag{40}$$

or using the logarithm of the attenuated backscatter coefficient :

$$\ln(\mathrm{U}(r)) = \ln(\beta(r)) - 2\int_0^r \alpha(r')dr' \tag{41}$$

From Eq.43, the extinction coefficient can be retrieved from the gradient as,

$$\alpha(r) = -\frac{1}{2}\frac{d}{dr}(\ln(\mathrm{U}(r)) + \frac{d(\ln(\beta(r))}{dr} \tag{42}$$

Lidar inversion - Slope method

In case of homogeneously distributed aerosol profiles, the latter term is zero.

$$\alpha(r) = -\frac{1}{2}\frac{d(\ln(\mathrm{U}(r))}{dr} \tag{43}$$

In this case, the extinction can be easily retrieved from the slope of the range corrected signal or from the attenuated backscatter.

Lidar inversion - Methods with boundary conditions

The basis lies in using a part of the atmosphere with known backscatter properties, typically a clean aerosol-free upper atmosphere (Fernald-Klett). From the logarithm of the range corrected lidar signal :

$$\ln(\mathrm{RCS}(r)) = \ln(K_o) + \ln(O(r)) + \ln(\beta(r)) - 2\int_0^r \alpha(r')dr' \tag{44}$$

Here, the RCS can be replaced by the attenuated backscatter function as,

$$\ln(\mathrm{U}(r)) = \ln(\beta(r)) - 2\int_0^r \alpha(r')dr' \tag{45}$$

Thus,

$$\ln(\mathrm{U}(r)) - \ln(U(o)) = \ln\frac{\beta(r)}{\beta_0} - 2\int_{r_0}^r \alpha(r')dr' \tag{46}$$

Lidar inversion - Methods with boundary conditions

By differentiating with respect to the range r yields,

$$\frac{d}{dr}\ln(U(r)) = \frac{1}{\beta}\frac{d\beta(r)}{dr} - 2\alpha(r) \tag{47}$$

Using a relation between extinction and backscattering :

$$LR = \alpha(r)/\beta(r) \tag{48}$$

it becomes,

$$\frac{d}{dr}\ln(U(r)) = \frac{1}{\beta}\frac{d\beta(r)}{dr} - 2LR\beta(r) \tag{49}$$

Lidar inversion - Methods with boundary conditions

This nonlinear differential equation has the form of a Bernoulli differential equation. For a one-component atmosphere, the *forward* solution of this differential equation, introduced by Fernald, is

$$\beta(r) = \beta_{\text{aer}}(r) + \beta_{\text{mol}}(r) = \frac{\mathrm{U}(r)}{\frac{\mathrm{U}(r_0)}{\beta_0} - 2\int_{r_0}^{r} \mathrm{LR}(r')\mathrm{U}(r')\,\mathrm{d}r'}. \tag{50}$$

Lidar inversion - Methods with boundary conditions

However, this solution is unstable and shows singularities regarding an imprecise determination of β_0. A more stable *backward* solution was later introduced by Klett using a reference range r^* in the far-range as,

$$\beta(r) = \beta_{\text{aer}}(r) + \beta_{\text{mol}}(r) = \frac{\mathrm{U}(r)}{\frac{\mathrm{U}(r^*)}{\beta^*} + 2\int_r^{r^*} \mathrm{LR}(r')\mathrm{U}(r')\,\mathrm{d}r'}. \tag{51}$$

It is assumed that the atmospheric composition at the reference range r^* is purely molecular.

Lidar inversion - Methods with boundary conditions

The reference height must be chosen very care-fully because it has a large impact on the results of the backscatter retrievals. It should be a reference zone where the backscattering is known, i.e. a pure molecular or nearly aerosol-free zone where molecular scattering is dominant .

Usually, the reference height is chosen in the upper free troposphere. This process is often referred to as "Rayleigh fitting".

Lidar inversion - Methods with boundary conditions

For a two-components atmosphere (i.e. with aerosol and molecules), where the molecular lidar ratio $\mathrm{LR}_{\mathrm{mol}}$ is considered as known, this form is obtained by splitting the exponential term into two parts so that only the total backscattering coefficient appears :

$$\mathrm{U}(r) = \beta(r) \exp\left[-2\int_0^r \mathrm{LR}_{\mathrm{aer}}\beta(r')\,\mathrm{d}r'\right] \exp\left[-2\int_0^r (\mathrm{LR}_{\mathrm{mol}} - \mathrm{LR}_{\mathrm{aer}})\beta_{\mathrm{mol}}(r')\,\mathrm{d}r'\right]. \tag{52}$$

where β_{mol} is commonly predicted from Rayleigh theory using air density profiles. Thus, Eq. (57) can be further simplified via

$$\mathrm{V}(r) = \beta(r) \exp\left[-2\int_0^r \mathrm{LR}_{\mathrm{aer}}\beta(r')\,\mathrm{d}r'\right] \tag{53}$$

with units of inverse distance time inverse solid angle.

Lidar inversion - Methods with boundary conditions

Let us define $\mathrm{V}(r)$ as a modified attenuated backscattering function, as

$$\mathrm{V}(r) = \mathrm{U}(r) \exp\left[2 \int_{r_0}^{r} (\mathrm{LR}_{\mathrm{mol}} - \mathrm{LR}_{\mathrm{aer}}) \beta_{\mathrm{mol}}(r')\, \mathrm{d}r'\right]. \tag{54}$$

Now, the total backscatter coefficients is given as :

$$\beta(r) = \beta_{\mathrm{aer}}(r) + \beta_{\mathrm{mol}}(r) = \frac{\mathrm{V}(r)}{\frac{V(r_0)}{\beta_0} + 2 \int_{r}^{r_0} \mathrm{LR}_{\mathrm{aer}}(r')\mathrm{V}(r')\, \mathrm{d}r'}. \tag{55}$$

and the aerosol backscatter coefficient :

$$\beta_{\mathrm{aer}}(r) = \frac{\mathrm{V}(r)}{\frac{V(r_0)}{\beta_0} + 2 \int_{r}^{r_0} \mathrm{LR}_{\mathrm{aer}}(r')\mathrm{V}(r')\, \mathrm{d}r'} - \beta_{\mathrm{mol}}(r) \tag{56}$$

Lidar inversion - Methods without boundary conditions

The lidar equation is converted to a form with a single unknown using $\mathrm{LR}_{\mathrm{aer}}$.

With $\mathrm{LR}_{\mathrm{mol}}$ regarded as known, this form is obtained by splitting the exponential term into two parts so that only the total backscattering coefficient appears :

$$\mathrm{U}(r) = \beta(r) \exp\left[-2\int_0^r \mathrm{LR}_{\mathrm{aer}}\beta(r')\,\mathrm{d}r'\right] \exp\left[-2\int_0^r (\mathrm{LR}_{\mathrm{mol}} - \mathrm{LR}_{\mathrm{aer}})\beta_{\mathrm{mol}}(r')\,\mathrm{d}r'\right]. \qquad (57)$$

where β_{mol} is commonly predicted from Rayleigh theory using air density profiles.

Lidar inversion - Methods without boundary conditions

Thus, Eq. (57) can be further simplified via

$$\mathrm{V}(r) = \beta(r) \exp\left[-2 \int_0^r \mathrm{LR}_{\mathrm{aer}} \beta(r')\, \mathrm{d}r'\right] \tag{58}$$

with units of inverse distance time inverse solid angle. In Eq. (58), $\mathrm{V}(r)$ is a modified attenuated backscattering function, which is related to Eq. (57) as

$$\mathrm{V}(r) = \mathrm{U}(r) \exp\left[2 \int_0^r (\mathrm{LR}_{\mathrm{mol}} - \mathrm{LR}_{\mathrm{aer}}) \beta_{\mathrm{mol}}(r')\, \mathrm{d}r'\right]. \tag{59}$$

Lidar inversion - Methods without boundary conditions

Equation (58) now contains a single unknown, β, which yields an analytical solution [108] as :

$$\beta(r) = \beta_{\text{aer}}(r) + \beta_{\text{mol}}(r) = \frac{\mathrm{V}(r)}{1 - 2\,\mathrm{LR}_{\text{aer}} \displaystyle\int_0^r \mathrm{V}(r')\,\mathrm{d}r'}. \tag{60}$$

Lidar inversion - Methods without boundary conditions

Equation. (60), however, requires fine-scale evaluation of the exponential term in Eq. (59), which can become a source of growing numerical errors. The resolution adopted here is to simultaneously evaluate this term along with Eq. (58).
Following Ceolato [108], two admittance quantities, $T(r)$ and $W(r)$, are introduced

$$\mathrm{T}(r) = \frac{\mathrm{V}(r)}{\beta(r)} = \exp\left[-2\int_0^r \mathrm{LR}_{\mathrm{aer}}\beta(r')\,\mathrm{d}r'\right] \tag{61}$$

$$\mathrm{W}(r) = \frac{\mathrm{V}(r)}{\mathrm{U}(r)} = \exp\left[-2\int_0^r (\mathrm{LR}_{\mathrm{aer}} - \mathrm{LR}_{\mathrm{mol}})\beta_{\mathrm{mol}}(r')\,\mathrm{d}r'\right]. \tag{62}$$

Lidar inversion - Methods without boundary conditions

It can be seens as solutions to the system of coupled 1st-order partial differential equations

$$\begin{cases} \partial_r \mathrm{W}(r) = -2(\mathrm{LR}_{\mathrm{mol}} - \mathrm{LR}_{\mathrm{aer}})\beta_{\mathrm{mol}}(r)\mathrm{W}(r), \\ \partial_r \mathrm{T}(r) = -2\mathrm{LR}_{\mathrm{aer}}\mathrm{U}(r)\mathrm{W}(r), \\ \mathrm{T}(0) = \mathrm{W}(0) = 1. \end{cases} \tag{63}$$

Lidar inversion - Methods without boundary conditions

The system in Eq. (63) is solved and β_{aer} is given by

$$\beta_{\text{aer}}(r) = \frac{\mathrm{U}(r)\mathrm{W}(r)}{\mathrm{T}(r)} - \beta_{\text{mol}}(r). \tag{64}$$

Next, $\beta_{\text{aer}}(r)$ is used to calculate $n_{\text{o}}(r, R_g)$ and $m_{\text{o}}(r, R_g)$, respectively, as :

$$\beta_{\text{aer}}(r) = \int_{R_{\text{min}}}^{R_{\text{max}}} n_{\text{o}}(r, R_g) \mathrm{d}C_{\text{aer}}^{\text{bac}}(r, R_g)\, \mathrm{d}R_g \tag{65}$$

where $n_{\text{o}}(r, R_g)$ is the particle number concentration per unit volume for an isotropic scattering medium formed by an ensemble of randomly oriented BC aggregates with radius of gyration R_{g}.

Lidar inversion - Methods without boundary conditions

$$\mathrm{d}C_{\mathrm{aer}}^{\mathrm{bac}}(r, R_g) = \left.\frac{d\sigma^{\mathrm{sca}}(r, R_g)}{d\Omega}\right|_{\theta=\pi} \tag{66}$$

and has units of surface time inverse solid angle. For a given mass specific backscattering efficiency σ^{bac}, the mass concentration of BC particulate matter is :

$$m_{\mathrm{o}}(r, R) = \frac{\beta_{\mathrm{aer}}(r)}{\sigma^{\mathrm{bac}}}, \tag{67}$$

with units of mass time inverse volume mg^2/m^3. Note that σ^{bac} is defined from the mass specific extinction coefficient σ^{ext} and the lidar ratio for BC as :

$$\sigma^{\mathrm{bac}} = \frac{\sigma^{\mathrm{ext}}}{\mathrm{LR}_{\mathrm{aer}}} \tag{68}$$

angle and inverse mass [m^2/(sr· mg)].

5. Application : black carbon aerosols

Black carbon aerosols

- Black carbon (BC) aerosols, produced from incomplete combustion and consisting of ultra-fine soot monomers, significantly impact climate and health.
- BC aerosols are of particular interest due to their strong absorption of solar radiation, which can lead to warming of the atmosphere and surface, and their ability to act as cloud condensation nuclei, which can affect cloud formation and precipitation [109].
- Advanced remote-sensing techniques like elastic backscatter lidar (EBL) are needed for accurate characterization near emission sources [110, 111, 112, 113, 114, 115].

Short-range elastic backscatter lidar

- Up to now, elastic lidar remains seldom-used to investigate atmospheric aerosols at short-range with a spatial-resolution less than one meter. A recent need for such capability has been identified : to characterize aerosols close to their emission sources by decreasing the minimal measurement height [116, 117, 118].
- Such backscatter lidar profiles are useful for environment and air quality monitoring in order to improve the modeling accuracy of aerosol dispersion during events such as industrial plume emission [110, 114] or aerosol events in the atmospheric boundary layer [119, 111, 120, 112].
- Also, short-range micro-lidars are showing new possibilities for investigating light-scattering properties of aerosols, including extinction and backscattering, with high-spatial-resolution [121, 122, 113, 115].

Short-range elastic backscatter lidar - Principle

Colibri lidar is a forward-looking instrument based on the PSR-EBL technique. It employs a high repetition rate laser with picosecond pulses, which permits backscatter measurements with a millisecond time and centimeter range-resolution using the time-of-flight principle for distance determination.

This is in contrast to conventional lidar systems intended for atmospheric studies.

Short-range elastic backscatter lidar - Principle

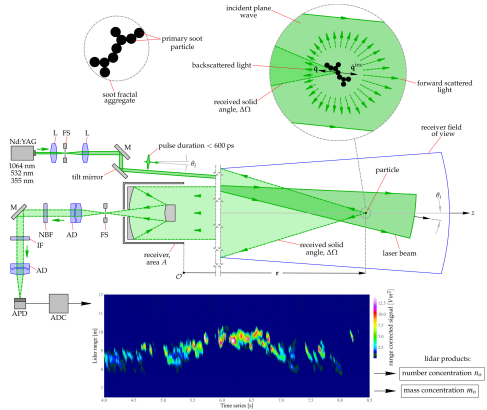

Figure – Principle of operation of the Picosecond Short-Range Elastic Backscatter Lidar (PSR-EBL)

Black Carbon Particles

BC particles are clusters of carbonaceous monomers with high graphite-like sp^2-bonded C atoms.

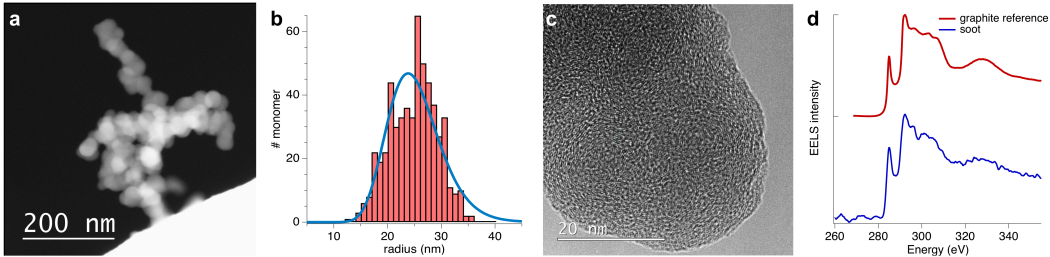

Figure – BC particles from a Jet-A1 pool-fire. (a) STEM/HAADF image of a BC aggregate. (b) Size distribution of the monomers (red bars) with lognormal fit. (c) HRTEM image of a monomer with an onion-like structure. (d) C-K edge EEL spectra of a monomer (blue) and graphite (red) as reference.

Rayleigh-Debye-Gans for Fractal Aggregates theory

Several accurate electromagnetic scattering methods simulate BC aggregates' radiative properties, but they are computationally intensive. The Rayleigh-Debye-Gans for Fractal Aggregates (RDG-FA) theory offers an accurate, analytical approximation for light-scattering, including lidar-relevant quantities, simplifying lidar inversion.

The RDG-FA theory, derived from Maxwell's equations, approximates light-scattering by BC aggregates. Despite assumptions like negligible monomer-monomer multiple scattering and uniform electromagnetic fields within monomers, it aligns well with experimental data due to interference cancellations.

Rayleigh-Debye-Gans for Fractal Aggregates theory

Provided that the lidar beam is vertically polarized and the received scattered light is also vertically polarized, the differential scattering cross-section $\mathrm{d}C_{\mathrm{bc}}^{\mathrm{sca,vv}}$ of a BC aggregate is proportional to the squared number of monomers N_{m}, the scattering cross-section of an individual monomer $\mathrm{d}C_{\mathrm{m}}^{\mathrm{sca,vv}}$, and a function f, called structure factor, that accounts for the fractal structure of the aggregate. The structure factor depends on R_{g}, the scattering angle θ, and the aggregate's fractal dimension D_{f}, thus

$$\mathrm{d}C^{\mathrm{sca,vv}} = N_{\mathrm{m}}^2 \, \mathrm{d}C_{\mathrm{m}}^{\mathrm{sca,vv}} f(R_{\mathrm{g}}, \theta, D_{\mathrm{f}}). \tag{69}$$

Rayleigh-Debye-Gans for Fractal Aggregates theory

We note that different expressions for f are reported in the literature [**?**, **?**]. Each formulation involves the scattering wave vector $q(\theta, \lambda) = (4\pi/\lambda)\sin(\theta/2)$. Here, we use that formulated by Dobbins and Megaridis[123] due to its simplicity and because it is known to be accurate at $\lambda = 532$ nm even when internal monomer-monomer multiple-scattering within the aggregate is considered :

$$f(R_g, \theta, D_f) = \begin{cases} \exp\left[\dfrac{-(qR_g)^2}{3}\right] & \text{if } (qR_g)^2 < \dfrac{3}{2}D_f \\ \left[\dfrac{3D_f}{2e(qR_g)^2}\right]^{\frac{D_f}{2}} & \text{if } (qR_g)^2 > \dfrac{3}{2}D_f \end{cases} \tag{70}$$

where it is understood that q is a function of θ and λ. For aerosols made of large clusters, only the power-law regime can be considered (second part of Eq. 70).

Rayleigh-Debye-Gans for Fractal Aggregates theory

Based on these expressions, the simplest analytical expression for the backscattering cross-section can then be found as :

$$\mathrm{d}C_{\mathrm{aer}}^{\mathrm{bac}} = N_{\mathrm{m}}^2 \frac{16\pi^4 R_{\mathrm{m}}^6}{\lambda^4} F(m) f^{\mathrm{bac}} C_{\mathrm{p}} \tag{71}$$

where $F(m) = \left|(m^2-1)/(m^2+2)\right|^2$, $f^{\mathrm{bac}} = f(R_{\mathrm{g}}, \theta = \pi, D_{\mathrm{f}})$ and C_{p} is a correction factor depending on the width of the aggregate-size distribution.

Rayleigh-Debye-Gans for Fractal Aggregates theory

An analytical expression of the lidar ratio can also be found as :

$$LR_{\mathrm{bc}} = \frac{\mathrm{d}C_{\mathrm{aer}}^{\mathrm{bac}}}{\mathrm{d}C^{\mathrm{ext}}} = \frac{\lambda^3}{2\pi^2 N_{\mathrm{m}} R_{\mathrm{m}}^3 f^{\mathrm{bac}}} \frac{E(m)}{F(m)} + \frac{8\pi}{3} \frac{g}{f^{\mathrm{bac}}} \tag{72}$$

which has units of solid angle and where $E(m) = \mathrm{Im}\left\{(m^2-1)/(m^2+2)\right\}$ and g is a correction factor also provided by Dobbins and Megaridis[123] as :

$$g = \left[1 + \frac{4}{3D_{\mathrm{f}}}\left(\frac{2\pi R_{\mathrm{g}}}{\lambda}\right)^2\right]^{-\frac{D_{\mathrm{f}}}{2}}. \tag{73}$$

Results

(i) The first-level products are the attenuated backscatter profiles $U(r, t)$ of Eq. (**??**), which are the range corrected lidar signals resulting from the application of a radiometric calibration[108]. The lidar signals are pre-processed to increase the signal-to-noise ratio. Here, this pre-processing consists of a dark current correction (DC), a background correction (BG), and a low pass filtering method that preserves the range resolution of the original signal.

(ii) The second-level products are backscatter profiles $\beta(r, t)$ obtained from a forward lidar-inversion method applied directly to the $U(r, t)$ signals. The inversion uses a light-scattering model that accounts for the fractal morphology of BC aerosols and is an essential element in determining accurate backscatter profiles from PSR-EBL technique. Here, the lidar ratio is calculated using the Rayleigh-Debye-Gans for Fractal Aggregates (RDG-FA) theory and the microphysical parameters provided by the STEM/HAADF analysis.

Results

(iii) Lastly, third-level products are the BC aerosols number and mass concentration range and time-dependent profiles $n_0(r,t)$ and $m_0(r,t)$. These are calculated using, respectively, the differential backscattering cross-section $\mathrm{d}C_{\mathrm{aer}}^{\mathrm{bac}}$ and mass-specific backscattering efficiency σ^{bac} for BC fractal aggregates via RDG-FA theory.

Results

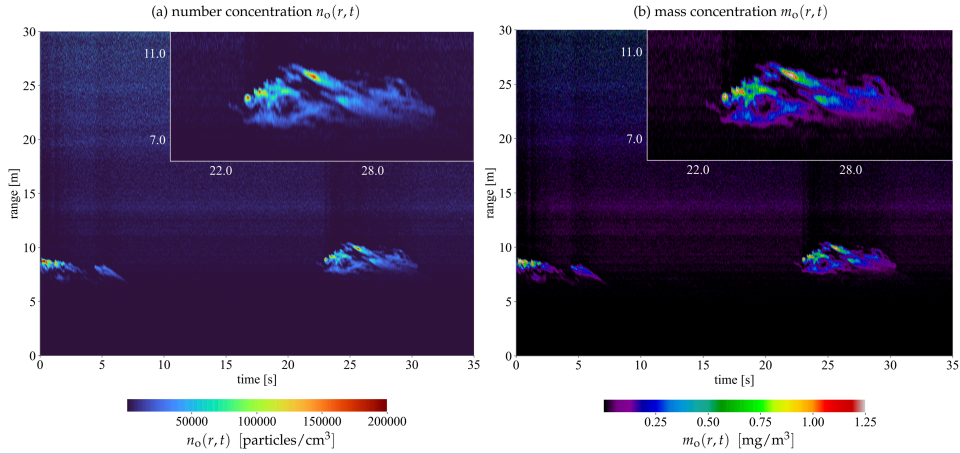
(a) number concentration $n_o(r,t)$
(b) mass concentration $m_o(r,t)$
range [m]
time [s]
11.0
7.0
22.0
28.0
50000
100000
150000
200000
$n_o(r,t)$ [particles/cm^3]
0.25
0.50
0.75
1.00
1.25
$m_o(r,t)$ [mg/m^3]

Results

- Range and time-resolved number $n_0(r, t)$ and mass $m_0(r, t)$ concentration profiles from the PSR-EBL technique of BC aerosols emitted by a small-scale Jet A-1 pool-fire.
- To highlight the resolution obtained, the inset images show a magnified view of the plume occurring violet between 20-30 s.
- The profiles are obtained using the RDG-FA theory and the microphysical parameters provided by the STEM/HAADF analysis.
- The profiles show the evolution of the BC aerosols in the plume, with the number and mass concentrations peaking at the center of the plume and decreasing towards the edges.
- The profiles also show the high spatial resolution of the PSR-EBL technique, which can resolve the plume structure with a resolution of 10 cm.

Thank you for your attention !

Any questions ?

www.onera.fr

References

[1] Z. Liu, A. Omar, M. Vaughan, J. Hair, C. Kittaka, Y. Hu, K. Powell, C. Trepte, D. Winker, C. Hostetler, R. Ferrare et R. Pierce,
CALIPSO lidar observations of the optical properties of Saharan dust : A case study of long-range transport,
Journal of Geophysical Research : Atmospheres, 113, (2008).

[2] M. Sicard, F. Molero, J. L. Guerrero-Rascado, R. Pedros, F. J. Exposito, C. Cordoba-Jabonero, J. M. Bolarin, A. Comeron, F. Rocadenbosch, M. Pujadas, L. Alados-Arboledas, J. A. Martinez-Lozano, J. P. Diaz, M. Gil, A. Requena, F. Navas-Guzman et J. M. Moreno,
Aerosol Lidar Intercomparison in the Framework of SPALINET—The Spanish Lidar Network : Methodology and Results,
IEEE Transactions on Geoscience and Remote Sensing, 47 (10), pp. 3547–3559 (2009).

[3] S. P. Burton, R. A. Ferrare, C. A. Hostetler, J. W. Hair, R. R. Rogers, M. D. Obland, C. F. Butler, A. L. Cook, D. B. Harper et K. D. Froyd,
Aerosol classification using airborne High Spectral Resolution Lidar measurements – methodology and examples,
Atmospheric Measurement Techniques, 5 (1), pp. 73–98 (2012).

[4] G. Pappalardo, A. Amodeo, M. Pandolfi, U. Wandinger, A. Ansmann, J. Bösenberg, V. Matthias, V. Amiridis, F. D. Tomasi, M. Frioud, M. Iarlori, L. Komguem, A. Papayannis, F. Rocadenbosch et X. Wang,
Aerosol lidar intercomparison in the framework of the EARLINET project. 3. Ramanlidar algorithm for aerosol extinction, backscatter, and lidar ratio,
Appl. Opt., 43 (28), pp. 5370–5385 (Oct 2004).

[5] A. J. Brown, G. Videen, E. Zubko, N. Heavens, N.-J. Schlegel, P. Beccera, C. Meyer, T. Harrison, P. Hayne, R. Obbard et et al.,
The case for a multi-channel polarization sensitive LIDAR for investigation of insolation-driven ices and atmospheres Planetary Science Decadal Survey White Paper,
Earth and Space Science Open Archive, p. 12 (2020).

[6] E. A. Johnson, R. C. Meyer, R. E. Hopkins et W. H. Mock,
The Measurement of Light Scattered by the Upper Atmosphere from a Search-Light Beam,
J. Opt. Soc. Am., 29 (12), pp. 512–517 (Dec 1939).

[7] R. Bureau,
Altimétrie des nuages par impulsions lumineuses,
Météorologie, (3), p. 292 (Jul. 1946).

[8] W. E. K. Middleton et A. F. Spilhaus,
Meteorological Instruments,
University of Toronto Press (1953).

[9] G. Fiocco et L. Smullin,
Detection of scattering layers in the upper atmosphere (60–140 km) by optical radar,
Nature, 199 (4900), pp. 1275–1276 (1963).

[10] H. Inaba et T. Kobayasi,
Laser-Raman Radar for Chemical Analysis of Polluted Air,
Nature, 224, pp. 170–2 (@nov 1969).

[11] V. Zuev,
Lidar Activity in Russia,
The Review of Laser Engineering, 23 (2), pp. 184–187 (1995).

[12] V. Zuev et J. Wood,
Laser Beams in the Atmosphere,
Consultants Bureau (1982).

[13] R. M. Measures,
Laser remote sensing : Fundamentals and applications,
New York, Wiley-Interscience (1984).

[14] P. C. Waterman,
Matrix formulation of electromagnetic scattering,
Proceedings of the IEEE, 53 (8), pp. 805–812 (1965).

[15] M. I. Mishchenko, L. D. Travis et D. W. Mackowski,
T-matrix computations of light scattering by nonspherical particles : A review,
Journal of Quantitative Spectroscopy and Radiative Transfer, 55 (5), pp. 535 – 575 (1996).

[16] M. Mishchenko et P. Martin,
Peter Waterman and T-matrix methods,
Journal of Quantitative Spectroscopy and Radiative Transfer, 123, pp. 2 – 7 (2013).

[17] L. Paulien, R. Ceolato, L. Soucasse, F. Enguehard et A. Soufiani,
Lidar-relevant radiative properties of soot fractal aggregate ensembles,
Journal of Quantitative Spectroscopy and Radiative Transfer, 241, p. 106706 (2020).

[18] R. Ceolato, L. Paulien, J. B. Maughan, C. M. Sorensen et M. J. Berg,
Radiative properties of soot fractal superaggregates including backscattering and depolarization,
Journal of Quantitative Spectroscopy and Radiative Transfer, 247, p. 106940 (2020).

[19] E. M. Purcell et C. R. Pennypacker,
Scattering and Absorption of Light by Nonspherical Dielectric Grains,
apj, 186, pp. 705–714 (décembre 1973).

[20] B. T. Draine et P. J. Flatau,
Discrete-Dipole Approximation For Scattering Calculations,
J. Opt. Soc. Am. A, 11 (4), pp. 1491–1499 (Apr 1994).

[21] M. Yurkin et A. Hoekstra,
The discrete dipole approximation : An overview and recent developments,
Journal of Quantitative Spectroscopy and Radiative Transfer, 106 (1), pp. 558 – 589 (2007).

[22] M. J. Berg et C. M. Sorensen,
Internal fields of soot fractal aggregates,
J. Opt. Soc. Am. A, 30 (10), pp. 1947–1955 (Oct 2013).

[23] R. Ceolato, F. Gaudfrin, O. Pujol, N. Riviere, M. J. Berg et C. M. Sorensen,
Lidar cross-sections of soot fractal aggregates : Assessment of equivalent-sphere models,
Journal of Quantitative Spectroscopy and Radiative Transfer, 212, pp. 39 – 44 (2018).

[24] S. A. Wood,
Identification of aerosol composition from multi-wavelength lidar measurements,
Technical Report, (NAS 1.26 :173445) (1984).

[25] H. Müller et H. Quenzel,
Information content of multispectral lidar measurements with respect to the aerosol size distribution,
Appl. Opt., 24 (5), pp. 648–654 (Mar 1985).

[26] P. Qing, H. Nakane, Y. Sasano et S. Kitamura,
Numerical simulation of the retrieval of aerosol size distribution from multiwavelength laser radar measurements,
Appl. Opt., 28 (24), pp. 5259–5265 (Dec 1989).

[27] Y. Sasano et E. V. Browell,
Light scattering characteristics of various aerosol types derived from multiple wavelength lidar observations,
Appl. Opt., 28 (9), pp. 1670–1679 (May 1989).

[28] R. H. Couch, C. W. Rowland, K. S. Ellis, M. P. Blythe, C. R. Regan, M. R. Koch, C. W. A. Jr., W. L. Kitchen, J. W. Cox, J. F. DeLorme, S. K. Crockett, R. G. Remus, J. C. Casas et W. H. Hunt,
Lidar In-Space Technology Experiment (LITE) : NASA's first in-space lidar system for atmospheric research,
Optical Engineering, 30 (1), pp. 88 – 95 (1991).

[29] M. J. Post, C. J. Grund, A. O. Langford et M. H. Proffitt,
Observations of Pinatubo ejecta over Boulder, Colorado by lidars of three different wavelengths,
Geophysical Research Letters, 19 (2), pp. 195–198 (1992).

[30] M. D. Guasta, M. Morandi, L. Stefanutti, B. Stein et J. P. Wolf,
Derivation of Mount Pinatubo stratospheric aerosol mean size distribution by means of a multiwavelength lidar,
Appl. Opt., 33 (24), pp. 5690–5697 (Aug 1994).

[31] H. Yoshiyama, A. Ohi et K. Ohta,
Derivation of the aerosol size distribution from a bistatic system of a multiwavelength laser with the singular value decomposition method,
Appl. Opt., 35 (15), pp. 2642–2648 (May 1996).

[32] K. Rajeev et K. Parameswaran,
Iterative method for the inversion of multiwavelength lidar signals to determine aerosol size distribution,
Appl. Opt., 37 (21), pp. 4690–4700 (Jul 1998).

[33] D. A. Ligon, J. B. Gillespie et P. Pellegrino,
Aerosol properties from spectral extinction and backscatter estimated by an inverse Monte Carlo method,
Appl. Opt., 39 (24), pp. 4402–4410 (Aug 2000).

[34] A. K. Jagodnicka, T. Stacewicz, G. Karasiński, M. Posyniak et S. P. Malinowski,
Particle size distribution retrieval from multiwavelength lidar signals for droplet aerosol,
Appl. Opt., 48 (4), pp. B8–B16 (Feb 2009).

[35] D. Müller, U. Wandinger, D. Althausen, I. Mattis et A. Ansmann,
Retrieval of physical particle properties from lidar observations of extinction and backscatter at multiple wavelengths,
Appl. Opt., 37 (12), pp. 2260–2263 (Apr 1998).

[36] D. Müller, F. Wagner, U. Wandinger, A. Ansmann, M. Wendisch, D. Althausen et W. von Hoyningen-Huene,
Microphysical particle parameters from extinction and backscatter lidar data by inversion with regularization : experiment,
Appl. Opt., 39 (12), pp. 1879–1892 (Apr 2000).

[37] I. Veselovskii, A. Kolgotin, D. Müller et D. N. Whiteman,
Information content of multiwavelength lidar data with respect to microphysical particle properties derived from eigenvalue analysis,
Appl. Opt., 44 (25), pp. 5292–5303 (Sep 2005).

[38] R. M. Schotland, K. Sassen et R. Stone,
Observations by Lidar of Linear Depolarization Ratios for Hydrometeors,
Journal of Applied Meteorology (1962-1982), 10 (5), pp. 1011–1017 (1971).

[39] S. R. Pal et A. I. Carswell,
Polarization Properties of Lidar Backscattering from Clouds,
Appl. Opt., 12 (7), pp. 1530–1535 (Jul 1973).

[40] K. Sassen,
The Polarization Lidar Technique for Cloud Research : A Review and Current Assessment,
Bulletin of the American Meteorological Society, 72 (12), pp. 1848–1866 (@dec 1991).

[41] M. I. Mishchenko et K. Sassen,
Depolarization of lidar returns by small ice crystals : An application to contrails,
Geophysical Research Letters, 25 (3), pp. 309–312 (1998).

[42] A. Ansmann, I. Mattis, D. Müller, U. Wandinger, M. Radlach, D. Althausen et R. Damoah,
Ice formation in Saharan dust over central Europe observed with temperature/humidity/aerosol Raman lidar,
Journal of Geophysical Research : Atmospheres, 110 (D18) (2005).

[43] K. Sassen, J. Zhu, P. Webley, K. Dean et P. Cobb,
Volcanic ash plume identification using polarization lidar : Augustine eruption, Alaska,
Geophysical Research Letters, 34 (8) (2007).

[44] G. P. Gobbi, F. Barnaba, R. Giorgi et A. Santacasa,
Altitude-resolved properties of a Saharan dust event over the Mediterranean,
Atmospheric Environment, 34 (29), pp. 5119 – 5127 (2000).

[45] M. Haarig, A. Ansmann, H. Baars, C. Jimenez, I. Veselovskii, R. Engelmann et D. Althausen,
Depolarization and lidar ratios at 355, 532, and 1064 nm and microphysical properties of aged tropospheric and stratospheric Canadian wildfire smoke,
Atmospheric Chemistry and Physics, 18 (16), pp. 11847–11861 (2018).

[46] V. Freudenthaler, F. Homburg et H. Jäger,
Optical parameters of contrails from lidar measurements : Linear depolarization,
Geophysical Research Letters, 23 (25), pp. 3715–3718 (1996).

[47] J. M. Richardson, J. C. Aldridge et A. B. Milstein,
Polarimetric lidar signatures for remote detection of biological warfare agents,
Dans *Polarization : Measurement, Analysis, and Remote Sensing VIII*, sous la direction de D. B. Chenault et D. H. Goldstein, vol. 6972, pp. 108 – 118. International Society for Optics and Photonics, SPIE (2008).

[48] D. Althausen, D. Müller, A. Ansmann, U. Wandinger, H. Hube, E. Clauder et S. Zörner,
Scanning 6-Wavelength 11-Channel Aerosol Lidar,
Journal of Atmospheric and Oceanic Technology, 17 (11), pp. 1469–1482 (@nov 2000).

[49] I. Veselovskii, A. Kolgotin, V. Griaznov, D. Müller, U. Wandinger et D. N. Whiteman,
Inversion with regularization for the retrieval of tropospheric aerosol parameters from multiwavelength lidar sounding,
Appl. Opt., 41 (18), pp. 3685–3699 (Jun 2002).

[50] N. Sugimoto et C. H. Lee,
Characteristics of dust aerosols inferred from lidar depolarization measurements at two wavelengths,
Appl. Opt., 45 (28), pp. 7468–7474 (Oct 2006).

[51] T. Sakai, T. Nagai, T. Kobayashi, A. Yamazaki, A. Uchiyama et Y. Mano,
Multiwavelength and polarization lidar measurements of Asian dust layers over Tsukuba, Japan : a case study,
Atmospheric Chemistry and Physics Discussions, 7, pp. 10179–10203 (2007).

[52] M. Wiegner, J. Gasteiger, K. Kandler, B. Weinzierl, K. Rasp, M. Esselborn, V. Freudenthaler, B. Heese, C. Toledano, M. Tesche et D. Althausen,
Numerical simulations of optical properties of Saharan dust aerosols with emphasis on lidar applications,
Tellus B : Chemical and Physical Meteorology, 61 (1), pp. 180–194 (2009).

[53] L. R. Bissonnette,
Lidar : Range-Resolved Optical Remote Sensing of the Atmosphere,
Chap. Lidar and Multiple Scattering, pp. 43–103. Springer New York, New York, NY (2005).

[54] M. I. Mishchenko,
Vector radiative transfer equation for arbitrarily shaped and arbitrarily oriented particles : a microphysical derivation from statistical electromagnetics,
Appl. Opt., 41 (33), pp. 7114–7134 (Nov 2002).

[55] F. G. Fernald, B. M. Herman et J. A. Reagan,
Determination of aerosol height distributions by lidar,
Journal of Applied meteorology, 11 (3), pp. 482–489 (1972).

[56] J. D. Klett,
Stable analytical inversion solution for processing lidar returns,
Applied optics, 20 (2), pp. 211–220 (1981).

[57] F. G. Fernald,
Analysis of atmospheric lidar observations : some comments,
Applied optics, 23 (5), pp. 652–653 (1984).

[58] T. Anderson, D. Covert, J. Wheeler, J. Harris, K. Perry, B. Trost, D. Jaffe et J. Ogren,
Aerosol backscatter fraction and single scattering albedo : Measured values and uncertainties at a coastal station in the Pacific Northwest,
Journal of Geophysical Research : Atmospheres, 104 (D21), pp. 26793–26807 (1999).

[59] C. Cattrall, J. Reagan, K. Thome et O. Dubovik,
Variability of aerosol and spectral lidar and backscatter and extinction ratios of key aerosol types derived from selected Aerosol Robotic Network locations,
Journal of Geophysical Research : Atmospheres, 110 (D10) (2005).

[60] F. Barnaba et G. P. Gobbi,
Modeling the aerosol extinction versus backscatter relationship for lidar applications : maritime and continental conditions,
Journal of Atmospheric and Oceanic Technology, 21 (3), pp. 428–442 (2004).

[61] F. Kanngiesser et M. Kahnert,
Coating material-dependent differences in modelled lidar-measurable quantities for heavily coated soot particles,
Opt. Express, 27 (25), pp. 36368–36387 (Dec 2019).

[62] H. Hulst et H. van de Hulst,
Light Scattering by Small Particles,
Dover Books on Physics. Dover Publications (1981).

[63] C. Bohren et D. R. Huffman,
Absorption and Scattering of Light by Small Particles,
Wiley (1983).

[64] M. I. Mishchenko, L. D. Travis et A. A. Lacis,
Scattering, absorption, and emission of light by small particles,
Cambridge university press (2002).

[65] M. J. Berg, C. M. Sorensen et A. Chakrabarti,
Extinction and the optical theorem. Part I. Single particles,
J. Opt. Soc. Am. A, 25 (7), pp. 1504–1513 (Jul 2008).

[66] G. Mie,
Beiträge zur Optik trüber Medien, speziell kolloidaler Metallösungen,
Annalen der Physik, 330 (3), pp. 377–445 (1908).

[67] F. T. Gucker, J. Tůma, H.-M. Lin, C.-M. Huang, S. C. Ems et T. R. Marshall,
Rapid measurement of light-scattering diagrams from single particles in an aerosol stream and determination of latex particle size,
Journal of Aerosol Science, 4 (5), pp. 389 – 404 (1973).

[68] M. Bartholdi, G. C. Salzman, R. D. Hiebert et M. Kerker,
Differential light scattering photometer for rapid analysis of single particles in flow,
Appl. Opt., 19 (10), pp. 1573–1581 (May 1980).

[69] N. Y. Misconi, J. P. Oliver, K. F. Ratcliff, E. T. Rusk et W.-X. Wang,
Light scattering by laser levitated particles,
Appl. Opt., 29 (15), pp. 2276–2281 (May 1990).

[70] P. H. Kaye, E. Hirst, J. M. Clark et F. Micheli,
Airborne particle shape and size classification from spatial light scattering profiles,
Journal of Aerosol Science, 23 (6), pp. 597 – 611 (1992).

[71] K. Aptowicz, R. Pinnick, S. Hill, Y. Pan et R. Chang,
Optical scattering patterns from single urban aerosol particles at Adelphi, Maryland, USA : A classification relating to particle morphologies,
Journal of Geophysical Research : Atmospheres, 111 (D12) (2006).

[72] K. B. Aptowicz, Y.-L. Pan, S. D. Martin, E. Fernandez, R. K. Chang et R. G. Pinnick,
Decomposition of atmospheric aerosol phase function by particle size and asphericity from measurements of single particle optical scattering patterns,
J. Quant. Spectros. Radiat. Transfer, 131, pp. 13–23 (2013).

[73] M. J. Berg, S. C. Hill, Y.-L. Pan et G. Videen,
Two-dimensional Guinier analysis : Application to single aerosol particles in-flight,
Optics Express, 18, pp. 23343–23352 (2010).

[74] F. Ferri,
Use of a charge coupled device camera for low-angle elastic light scattering,
Rev. Sci. Instrum., 68, pp. 2265–2274 (1997).

[75] M. J. Berg, S. C. Hill, G. Videen et K. P. Gurton,
Spatial filtering technique to image and measure two-dimensional near-forward scattering from single particles,
Optics Express, 18, pp. 9486–9495 (2010).

[76] M. J. Berg, Y. W. Heinson, O. Kemppinen et S. Holler,
Solving the inverse problem for coarse-mode aerosol particle morphology with digital holography,
Sci. Rep., 7, p. 9400 (2017).

[77] R. Ceolato, K. Aleau, L. Paulien, F. Fossard, E. Reynoso-Lara et M. J. Berg,
Two-dimensional small-angle scattering from single particles in infrared with a lensless technique,
Opt. Express, 28 (17), pp. 25114–25122 (Aug 2020).

[78] M. J. Berg et G. Videen,
Digital holographic imaging of aerosol particles in flight,
Journal of Quantitative Spectroscopy and Radiative Transfer, 112 (11),
pp. 1776–1783 (2011).

[79] M. J. Berg, N. R. Subedi, P. A. Anderson et N. B. Fowler,
Using holography to measure extinction,
Opt. Lett., 39 (13), pp. 3993–3996 (Jul 2014).

[80] M. J. Berg, N. R. Subedi et P. A. Anderson,
Measuring extinction with digital holography : nonspherical particles and experimental validation,
Opt. Lett., 42 (5), pp. 1011–1014 (2017).

[81] M. J. Berg et C. Sorensen,
A review and reassessment of diffraction, scattering, and shadows in electrodynamics,
Journal of Quantitative Spectroscopy and Radiative Transfer, 210, pp. 225–239 (2018).

[82] M. J. Berg, C. M. Sorensen et A. Chakrabarti,
Extinction and the optical theorem. Part II. Multiple particles,
J. Opt. Soc. Am. A, 25 (7), pp. 1514–1520 (Jul 2008).

[83] D. Deirmendjian et R. Corporation,
Electromagnetic Scattering on Spherical Polydispersions,
R (Rand Corporation). American Elsevier Publishing Company (1969).

[84] Y. Xu,
Electromagnetic scattering by an aggregate of spheres : far field,
Appl. Opt., 36 (36), pp. 9496–9508 (Dec 1997).

[85] R. H. Zerull, B. Å. S. Gustafson, K. Schulz et E. Thiele-Corbach,
Scattering by aggregates with and without an absorbing mantle : microwave analog experiments,
Appl. Opt., 32 (21), pp. 4088–4100 (Jul 1993).

[86] L. Kolokolova et B. A. S. Gustafsonm,
Scattering by inhomogeneous particles : microwave analog experiments and comparison to effective medium theories,
Journal of Quantitative Spectroscopy and Radiative Transfer, 70 (4), pp. 611 – 625 (2001).

[87] R. Vaillon, J.-M. Geffrin, C. Eyraud, O. Merchiers, P. Sabouroux et B. Lacroix,
A new implementation of a microwave analog to light scattering measurement device,
Journal of Quantitative Spectroscopy and Radiative Transfer, 112 (11), pp. 1753 – 1760 (2011).

[88] J. P. Reid,
Particle levitation and laboratory scattering,
Journal of Quantitative Spectroscopy and Radiative Transfer, 110 (14-16), pp. 1293–1306 (2009).

[89] K. Sassen,
Optical backscattering from near-spherical water, ice, and mixed phase drops,
Appl. Opt., 16 (5), pp. 1332–1341 (May 1977).

[90] W. Szymanski, R. Rudolf et T. Ciach,
On the information content of the light backscattering and transmittance curves in aerosols,
Journal of aerosol science, 28 (7), pp. 1137–1147 (1997).

[91] T. Sakai, T. Nagai, Y. Zaizen et Y. Mano,
Backscattering linear depolarization ratio measurements of mineral, sea-salt, and ammonium sulfate particles simulated in a laboratory chamber,
Appl. Opt., 49 (23), pp. 4441–4449 (Aug 2010).

[92] A. Miffre, D. Cholleton et P. Rairoux,
Laboratory evaluation of the scattering matrix elements of mineral dust particles from 176.0 ° up to 180.0 °-exact backscattering angle,
Journal of Quantitative Spectroscopy and Radiative Transfer, 222-223, pp. 45 – 59 (2019).

[93] A. Miffre, T. Mehri, M. Francis et P. Rairoux,
UV–VIS depolarization from Arizona Test Dust particles at exact backscattering angle,
Journal of Quantitative Spectroscopy and Radiative Transfer, 169, pp. 79 – 90 (2016).

[94] R. Fu, C. Wang, O. Muñoz, G. Videen, J. L. Santarpia et Y.-L. Pan,
Elastic back-scattering patterns via particle surface roughness and orientation from single trapped airborne aerosol particles,
Journal of Quantitative Spectroscopy and Radiative Transfer, 187, pp. 224 – 231 (2017).

[95] Y.-L. Pan, C. Wang, L. A. Beresnev, A. J. Yuffa, G. Videen, D. Ligon et J. L. Santarpia,
Measurement of back-scattering patterns from single laser trapped aerosol particles in air,
Applied Optics, 56 (3), pp. B1–B4 (2017).

[96] E. W. Barrett et O. Ben-Dov,
Application of the Lidar to Air Pollution Measurements,
Journal of Applied Meteorology, 6 (3), pp. 500–515 (06 1967).

[97] R. T. H. Collis,
Lidar : A new atmospheric probe,
Quarterly Journal of the Royal Meteorological Society, 92 (392), pp. 220–230 (1966).

[98] W. Viezee, E. E. Uthe et R. T. H. Collis,
Lidar Observations of Airfield Approach Conditions :An Exploratory Study,
Journal of Applied Meteorology, 8 (2), pp. 274–283 (04 1969).

[99] W. Viezee, E. E. Uthe et R. T. H. Collis,
Lidar Observations of Airfield Approach Conditions :An Exploratory Study,
Journal of Applied Meteorology, 8 (2), pp. 274–283 (1969).

[100] Y. Sasano, E. V. Browell et S. Ismail,
Error caused by using a constant extinction/backscattering ratio in the lidar solution,
Appl. Opt., 24 (22), pp. 3929–3932 (Nov 1985).

[101] G. Roy, G. Vallée et M. Jean,
Lidar-inversion technique based on total integrated backscatter calibrated curves,
Appl. Opt., 32 (33), pp. 6754–6763 (Nov 1993).

[102] V. A. Kovalev,
Sensitivity of the lidar solution to errors of the aerosol backscatter-to-extinction ratio : influence of a monotonic change in the aerosol extinction coefficient,
Appl. Opt., 34 (18), pp. 3457–3462 (Jun 1995).

[103] S. T. Shipley, D. H. Tracy, E. W. Eloranta, J. T. Trauger, J. T. Sroga, F. L. Roesler et J. A. Weinman,
High spectral resolution lidar to measure optical scattering properties of atmospheric aerosols. 1 : Theory and instrumentation,
Appl. Opt., 22 (23), pp. 3716–3724 (Dec 1983).

[104] J. T. Sroga, E. W. Eloranta, S. T. Shipley, F. L. Roesler et P. J. Tryon,
High spectral resolution lidar to measure optical scattering properties of atmospheric aerosols. 2 : Calibration and data analysis,
Appl. Opt., 22 (23), pp. 3725–3732 (Dec 1983).

[105] E. E. Eloranta,
High spectral resolution lidar,
Dans *Lidar*, pp. 143–163. Springer (2005).

[106] J. Cooney,
Remote measurements of atmospheric water vapor profiles using the Raman component of laser backscatter,
Journal of Applied Meteorology, 9 (1), pp. 182–184 (1970).

[107] A. Ansmann, M. Riebesell et C. Weitkamp,
Measurement of atmospheric aerosol extinction profiles with a Raman lidar,
Opt. Lett., 15 (13), pp. 746–748 (Jul 1990).

[108] R. Ceolato, A. E. Bedoya-Velásquez et V. Mouysset,
Short-Range Elastic Backscatter Micro-Lidar for Quantitative Aerosol Profiling with High Range and Temporal Resolution,
Remote Sensing, 12 (20) (2020),
https://www.mdpi.com/2072-4292/12/20/3286.

[109] T. C. Bond, S. J. Doherty, D. W. Fahey, P. M. Forster, T. Berntsen, B. J. DeAngelo, M. G. Flanner, S. Ghan, B. Kärcher, D. Koch, S. Kinne, Y. Kondo, P. K. Quinn, M. C. Sarofim, M. G. Schultz, M. Schulz, C. Venkataraman, H. Zhang, S. Zhang, N. Bellouin, S. K. Guttikunda, P. K. Hopke, M. Z. Jacobson, J. W. Kaiser, Z. Klimont, U. Lohmann, J. P. Schwarz, D. Shindell, T. Storelvmo, S. G. Warren et C. S. Zender,
Bounding the role of black carbon in the climate system : A scientific assessment,
Journal of Geophysical Research : Atmospheres, 118 (11), pp. 5380–5552 (2013),
https://agupubs.onlinelibrary.wiley.com/doi/abs/10.1002/jgrd.50171.

[110] H. Edner, P. Ragnarson et E. Wallinder,
Industrial Emission Control Using Lidar Techniques,
Environmental Science & Technology, 29 (2), pp. 330–337 (1995).

[111] M. Schröter, A. Obermeier, D. Brüggemann, M. Plechschmidt et O. Klemm,
Remote Monitoring of Air Pollutant Emissions from Point Sources by a Mobile Lidar/Sodar System,
Journal of the Air & Waste Management Association, 53 (6), pp. 716–723 (2003).

[112] T. T. Evgenieva, N. I. Kolev, I. T. Iliev, P. B. Savov, B. K. Kaprielov, P. C. S. Devara et I. N. Kolev,
Lidar and spectroradiometer measurements of atmospheric aerosol optical characteristics over an urban area in Sofia, Bulgaria,
International Journal of Remote Sensing, 30 (24), pp. 6381–6401 (2009).

[113] D. M. Brown, E. Thrush et M. E. Thomas,
Chamber lidar measurements of biological aerosols,
Appl Opt, 50 (5), pp. 717–24 (2011).

[114] J. L. Guerrero-Rascado, R. F. da Costa, A. E. Bedoya, R. Guardani, L. Alados-Arboledas, Álvaro Efrain Bastidas et E. Landulfo,
Multispectral elastic scanning lidar for industrial flare research : characterizing the electronic subsystem and application,
Opt. Express, 22 (25), pp. 31063–31077 (Dec 2014).

[115] D. M. Brown, A. M. Brown, A. H. Willitsford, R. Dinello-Fass, M. B. Airola, K. M. Siegrist, M. E. Thomas et Y. Chang,
Lidar measurements of solid rocket propellant fire particle plumes,
Appl Opt, 55 (17), pp. 4657–69 (2016).

[116] E. J. Welton et J. R. Campbell,
Micropulse Lidar Signals : Uncertainty Analysis,
Journal of Atmospheric and Oceanic Technology, 19 (12), pp. 2089–2094 (@dec 2002).

[117] W. Gong, J. Li, F. Mao et J. Zhang,
Comparison of simultaneous signals obtained from a dual-field-of-view lidar and its application to noise reduction based on empirical mode decomposition,
Chin. Opt. Lett., 9 (5), p. 050101 (May 2011).

[118] P. M. Ong, N. Lagrosas, T. Shiina et H. Kuze,
Surface Aerosol Properties Studied Using a Near-Horizontal Lidar,
Atmosphere, 11 (1) (2019).

[119] M. Del Guasta,
Daily cycles in urban aerosols observed in Florence (Italy) by means of an automatic 532–1064nm LIDAR,
Atmospheric Environment, 36 (17), pp. 2853 – 2865 (2002).

[120] G. de Arruda Moreira, J. L. Guerrero-Rascado, J. A. Benavent-Oltra, P. Ortiz-Amezcua, R. Román, A. E. Bedoya-Velásquez, J. A. Bravo-Aranda, F. J. Olmo Reyes, E. Landulfo et L. Alados-Arboledas,
Analyzing the turbulent planetary boundary layer by remote sensing systems : the Doppler wind lidar, aerosol elastic lidar and microwave radiometer,
Atmospheric Chemistry and Physics, 19 (2), pp. 1263–1280 (2019).

[121] J. W. Giles, I. N. Bankman, R. M. Sova, T. R. Morgan, D. D. Duncan, J. A. Millard, W. J. Green et F. J. Marcotte,
Lidar system model for use with path obscurants and experimental validation,
Appl Opt, 47 (22), pp. 4085–93 (2008).

[122] G. Tremblay, X. Cao et G. Roy,
The effect of dense aerosol cloud on the 3D information contain of flash Lidar,
Proceedings of SPIE - The International Society for Optical Engineering, 7828 (@oct 2010).

[123] R. A. Dobbins et C. M. Megaridis,
Absorption and scattering of light by polydisperse aggregates,
Applied optics, 30 (33), pp. 4747–4754 (1991).